

## Article

# Individual and Joint Effect of Oleic Acid Imidazoline and $\text{CeCl}_3$ on Carbon Steel Corrosion in $\text{CO}_2$ -Saturated Brine Solution

Tihomir Borko<sup>1</sup>, Gordana Bilić<sup>2,\*</sup> , Katarina Žbulj<sup>2</sup>  and Helena Otmačić Ćurković<sup>3</sup> <sup>1</sup> INA, d.d., 10000 Zagreb, Croatia; tihomir.borko@ina.hr<sup>2</sup> Faculty of Mining, Geology and Petroleum Engineering, University of Zagreb, 10000 Zagreb, Croatia; katarina.zbulj@rgn.unizg.hr<sup>3</sup> Faculty of Chemical Engineering and Technology, University of Zagreb, 10000 Zagreb, Croatia; hotmac@fkit.unizg.hr

\* Correspondence: gordana.bilic@rgn.hr; Tel.: +385-1-5535-909

**Abstract:** In production and transportation systems of the oil industry, brine solutions contain high concentrations of chloride and dissolved  $\text{CO}_2$ , which is a very corrosive medium to which carbon steel is exposed. Therefore, finding new effective and environmentally friendly corrosion inhibitors is of great importance. The effect of  $\text{CeCl}_3$  (in concentrations from  $5 \text{ mg dm}^{-3}$  to  $20 \text{ mg dm}^{-3}$ ) and oleic acid imidazoline (IOA) (in concentrations from  $5 \text{ mg dm}^{-3}$  to  $20 \text{ mg dm}^{-3}$ ) separately and their mixtures (in concentrations from  $5 \text{ mg dm}^{-3}$  to  $15 \text{ mg dm}^{-3}$  of  $\text{CeCl}_3$  and from  $5 \text{ mg dm}^{-3}$  to  $20 \text{ mg dm}^{-3}$  of IOA) as corrosion inhibitors of AISI 1018 carbon steel corrosion in simulated brine solution saturated with  $\text{CO}_2$  at  $60^\circ\text{C}$  were examined by means of weight-loss testing, electrochemical measurements (polarization resistance, linear polarization with Tafel extrapolation, electrochemical impedance spectroscopy) and surface analyses (scanning electron microscopy with energy-dispersive X-ray spectroscopy analyses, Raman spectroscopy and X-ray diffraction). All test methods showed a higher efficiency of compounds' mixtures (from 62.77% to 97.94%) and a higher degree of corrosion protection compared to the action of individual compounds (efficiency from 3.43% to 94.61% for IOA and from 57.58% to 96.27% for  $\text{CeCl}_3$ ). Imidazoline, a common corrosion inhibitor in  $\text{CO}_2$ -saturated systems, most likely forms a surface film with voids via its adsorption on steel surface, while cerium carbonate tends to fill these voids by creating a more compact film. In this way, a denser and thicker surface film is formed.

**Keywords:**  $\text{CO}_2$  corrosion; corrosion inhibitor;  $\text{CeCl}_3$ ; oleic acid-based imidazoline; synergism



Academic Editor: Ludmila B. Boinovich

Received: 12 December 2024

Revised: 8 January 2025

Accepted: 12 January 2025

Published: 15 January 2025

**Citation:** Borko, T.; Bilić, G.; Žbulj, K.; Otmačić Ćurković, H. Individual and Joint Effect of Oleic Acid Imidazoline and  $\text{CeCl}_3$  on Carbon Steel Corrosion in  $\text{CO}_2$ -Saturated Brine Solution.

*Coatings* **2025**, *15*, 93. <https://doi.org/10.3390/coatings15010093>

**Copyright:** © 2025 by the authors.

Licensee MDPI, Basel, Switzerland.

This article is an open access article distributed under the terms and conditions of the Creative Commons Attribution (CC BY) license

(<https://creativecommons.org/licenses/by/4.0/>).

## 1. Introduction

Carbon capture, utilization and storage (CCUS) is considered an effective way of reducing  $\text{CO}_2$  emissions, and it is often used for enhanced oil recovery purposes ( $\text{CO}_2$ -EOR) [1–6]. It is known that the produced fluids are quite corrosive media (they contain oil, water, chlorides, acids and dissolved gases) that impair the integrity and useful properties of transportation pipelines and tubing [7–9].

In oil and gas production and transport pipelines, as well as in carbon capture storage systems, corrosion of the inner walls of the pipes, due to the presence of  $\text{CO}_2$ , results in pipeline rupture, the loss of production and transport fluid, economic losses and ecological disaster [10–14]. Situations are much worse when high chloride concentrations are present as well as turbulent hydrodynamic conditions [15].

Most pipelines for systems containing CO<sub>2</sub> (oil and gas production, geothermal systems, carbon capture, utilization and storage systems) are made of carbon steel. Although carbon steel is subject to corrosion in exposed conditions, the reason for its wide application is due to its favorable metallurgical properties as well as economic profitability [16–18].

One of the oldest and most common methods of protecting metals from corrosion is the application of corrosion inhibitors [19]. Corrosion inhibitors are defined as substances that, added in small amounts, slow down or prevent metal corrosion [20]. In the past, the only factor in selecting an inhibitor was its effectiveness, while its environmental impact was neglected. In addition, it was believed that effective corrosion inhibitors could not be environmentally friendly, and environmentally friendly compounds could not be effective corrosion inhibitors [21].

Fortunately, nowadays, the selection and application of corrosion inhibitors has moved from an exclusively economic aspect to taking into account environmental factors, i.e., it is necessary to satisfy the so-called E3 concept (efficiency, economy and ecology). Before 1960, the only criterion that had to be met when choosing an inhibitor was effectiveness, and the following were widely used: chromates, phosphates, nitrates, borates, silicates and zinc compounds. Although extremely effective as corrosion inhibitors and economically viable, today's chromates (like most inorganic inhibitors) are banned for health and safety reasons. From 1960 to 1980, the focus when choosing inhibitors was on the economic aspect; so polyphosphates, gluconates, vanadates, molybdates, carboxylates and surface-active chelates were used. Tannins, vitamins, natural compounds and polymers were widely used from 1980 to 1995 when ecology was the main required property of the inhibitor. From 1995 until today, inhibitors must be environmentally friendly, which is why compounds like rare earth metal compounds, multifunctional organic compounds, mixtures of rare earth metals and organic/inorganic compounds and the encapsulation of inhibitors are preferred [21,22].

Chemicals in the general sense, and thus non-ecological corrosion inhibitors, cause numerous environmental problems, which is why the development of “green chemistry” that also applies to corrosion inhibitors has occurred. “Green chemistry” refers to chemicals and chemical processes that reduce or eliminate the negative impact on the environment since they reduce waste products, do not contain toxic compounds and improve efficiency [23].

Scientists invest a lot of effort in finding and producing inhibitors that are both highly effective and low in toxicity. Such inhibitors are called “environmentally friendly”, “green inhibitors” or “environmentally acceptable inhibitors” [24,25].

In the eighties of the last century, the development of a new group of corrosion inhibitors, salts of rare earth metals (REM), began. Their development was slow, and they did not reach the importance of organic inhibitors despite their significant effectiveness. Among the rare earth salts, lanthanoids stand out as effective corrosion inhibitors. Cerium, praseodymium, neodymium, lanthanum and ytterbium ions showed very high inhibitory effectiveness on aluminum alloys [26,27].

Small animal studies of cerium compounds have shown low toxicity, which can be related to other lanthanides. Lanthanides are economically competitive products, and the relative prevalence of some of them (e.g., cerium) makes them additionally acceptable. The chemical properties of the lanthanides, for example the low solubility of their oxides and hydroxides, make them particularly suitable for corrosion inhibition [28–31]. Excellent corrosion inhibition is attributed to the high reactivity of rare earths. In the articles, the formation of a protective film and the inhibition of the cathodic corrosion reaction have been proven [32–37].

Imidazolines are a special class of corrosion inhibitors that have proven to be highly effective, and therefore, they have a wide range of applications in protection against CO<sub>2</sub>

corrosion. In addition to being highly effective in protecting against CO<sub>2</sub> corrosion, they are also available and environmentally friendly. To further improve their effectiveness, commercial forms of imidazolines are most often mixtures of imidazolines and other compounds, i.e., these are imidazoline derivatives [38]. Imidazoline derivatives are organic compounds based on nitrogen that act as cationic surfactants, depending on the nature of the hydrocarbon substituting group attached to the carbon or nitrogen atom of the imidazole ring [39]. The imidazoline head (with free electron pairs on nitrogen atoms and delocalized  $\pi$ -electrons) binds to the metal surface, while the hydrophobic tail represents a kind of barrier against the diffusion of water ions [40]. The inhibitory effect is attributed to physical (electrostatic interaction of the inhibitor molecule and the metal) or chemical adsorption (sharing or transfer of electrons between the inhibitor and the metal) on the metal surface, resulting in the formation of a protective film [39].

The examination of the synergistic effect of the compounds is carried out with the assumption of an increase in the inhibitory effectiveness in corrosion protection, as well as due to a reduction in the doses of chemicals [38,41–46]. The synergistic action involving rare earth metal salts as corrosion inhibitors is rarely investigated; therefore, the aim of this work is to examine the potentially synergistic action of rare earth salt, CeCl<sub>3</sub> and imidazoline based compounds.

In this work, the joint/synergistic effect of cerium chloride and imidazoline on the corrosion of carbon steel in a simulated brine solution saturated with CO<sub>2</sub> at 60 °C (which corresponds to the average temperature of the transported fluid in the oil industry) was tested. The inhibitory action of individual components as well as their synergistic action was tested using the mass loss method as well as the electrochemical methods of potentiodynamic polarization, measurement of polarization resistance and electrochemical impedance spectroscopy. The surface analysis of carbon steel samples was examined using scanning electron microscopy with energy-dispersive spectroscopy, X-ray diffraction and Raman spectroscopy.

## 2. Materials and Methods

The tested alloy is the AISI 1018 carbon steel with the chemical composition determined via optical emission spectrometry on a GDS 850 Leco spectrophotometer, MI, USA, and it is composed of the following (wt.%): 0.35 C, 0.35 Si, 1.09 Mn, 0.007 P, 0.024 S, 0.09 Cr, 0.07 Ni, 0.01 Mo, 0.10 Cu, <0.01 V and Fe balance. The steel has a ferrite–pearlite microstructure, as shown in Figure 1.

The carbon steel surface area for tests using the mass loss method was 23.72 cm<sup>2</sup>, while for electrochemical tests, the surface area exposed to the action of the tested electrolyte was 1 cm<sup>2</sup>. Before testing, the carbon steel samples were wet sanded with a silicon carbide abrasive paper up to 1200 grit, washed with double distilled water, degreased in 96% ethanol and dried in a stream of air.

The tested electrolyte is composed of 800 mL of chloride–carbonate solution (synthetic brine solution, SBS) saturated with CO<sub>2</sub>, both without and with inhibitors (individually and in a mixture). The chloride–carbonate solution was prepared by dissolving 30.0 g dm<sup>-3</sup> NaCl, 0.1 g dm<sup>-3</sup> NaHCO<sub>3</sub> and 0.1 g dm<sup>-3</sup> CaCO<sub>3</sub> in distilled water. The chloride–carbonate solution was saturated with CO<sub>2</sub> by bubbling CO<sub>2</sub> for 1 h before the start of the measurement and continued during the experiment. The composition of the tested electrolyte corresponds to the composition of natural, stratified waters of oil deposits in Croatia, except that the chloride content has been increased to carry out corrosion tests under severe conditions. The pH value of the prepared solution was 5.3. The pH value was measured with a Portable Waterproof pH meter HI991300, Hanna Instruments, Bedfordshire, UK, (pH accuracy  $\pm 0.1$  pH, pH range 0.0–14.0). The chemicals used for the

preparation of simulated brine solution were analytical grade and produced by Sigma Aldrich, Darmstadt, Germany. In the experiment, imidazoline oleic acid (IOA), produced by Sigma Aldrich, Darmstadt, Germany, and cerium chloride, also produced by Sigma Aldrich, Darmstadt, Germany, as corrosion inhibitors were used. The chemical structures of imidazoline based on oleic acid and cerium chloride are shown in Figure 2.

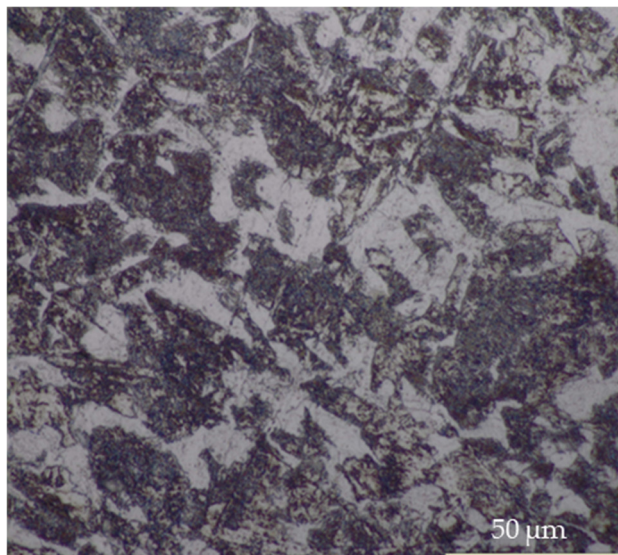


**Figure 1.** The ferrite–pearlite microstructure of the tested AISI 1018 carbon steel scanned with an Olympus GX51 light microscope, Tokyo, Japan, magnification 1000 $\times$ .

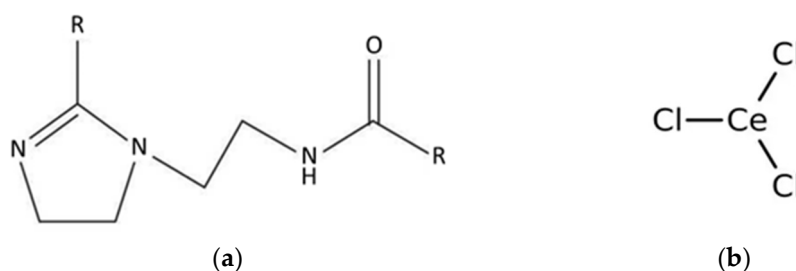


**Figure 2.** Chemical structures of (a) oleic acid imidazoline-based compound and (b) cerium chloride anhydride.

Both tested compounds were added individually in concentrations of 5 mg dm<sup>-3</sup>, 10 mg dm<sup>-3</sup>, 15 mg dm<sup>-3</sup> and 20 mg dm<sup>-3</sup>, while the inhibitor mixture consisted of 5 mg dm<sup>-3</sup>, 10 mg dm<sup>-3</sup>, 15 mg dm<sup>-3</sup> or 20 mg dm<sup>-3</sup> IOA with the addition of 5 mg dm<sup>-3</sup>, 10 mg dm<sup>-3</sup> or 15 mg dm<sup>-3</sup> CeCl<sub>3</sub> to each of these concentrations. The concentrations of individual components used in this work are arbitrary and lower than those reported in the literature for similar test systems. The aim in selecting concentrations was to achieve satisfactory efficacy at as low a concentration of individual components and as low a concentration of their mixtures as possible, i.e., use the lowest possible doses of chemicals.

All measurements were carried out at a temperature of 60  $\pm$  1  $^{\circ}$ C with stirring at a speed of 300 rpm; they were repeated at least three times, and very good reproducibility of the results was achieved (relative standard deviation was less than 5%).

### 2.1. Mass Loss Measurements

Tests using the mass loss method were performed in accordance with the ASTM G-1 standard. Before immersion in the tested electrolyte, the steel coupons were prepared in the previously described manner (treated with sandpaper, washed, degreased and dried)

and weighed on an analytical balance with an accuracy of  $\pm 0.1$  mg. After 72 h of exposure to the tested electrolytes, the coupons were taken out, and their surfaces were cleaned with a Clarke's solution (ASTM G 1-03 pickling solution consists of 5% stannous chloride and 2% antimony trioxide in concentrated hydrochloric acid), washed with distilled water, degreased with 96% ethanol, dried in a stream of air and weighed again on an analytical balance. The chemicals used for the preparation of Clarke's solution and the ethanol used for degreasing were analytical grade and produced by Sigma Aldrich, Darmstadt, Germany. All tests were performed at least four times, and very good reproducibility of the obtained measurement results was achieved.

## 2.2. Electrochemical Measurements

Electrochemical corrosion tests were performed on an EG&G PAR 378 potentiostat/galvanostat, IL, USA, in conjunction with the Power Suite software 2.41. An electrochemical cell with a three-electrode system was connected to the potentiostat. The working electrode was a sample of tested carbon steel AISI 1018, with a circular cross-section, inserted into the holder of the working electrode, so that the surface of the steel exposed to the action of the electrolyte was  $1 \text{ cm}^2$ . A saturated calomel electrode was used for the reference electrode, and two graphite rods were used for the counter electrodes.

The electrochemical measurements were performed after 24 h of stabilization of the working electrode at the open circuit potential.

Linear polarization curves in a narrow range of potential were recorded,  $\pm 10$  mV in relation to the open circuit potential with a scanning rate of  $0.1660 \text{ mV s}^{-1}$ , from which the polarization resistances were determined.

Potentiodynamic polarization recordings were performed in a potential range of  $\pm 250$  mV in relation to the open circuit potential with a scanning rate of  $0.1660 \text{ mV s}^{-1}$ . Corrosion rates were calculated using the Tafel extrapolation method. The method includes extrapolation of the linear cathodic and linear anodic parts of the polarization curve to their intersection, which corresponds to the corrosion current and corrosion potential from which the software calculates the corrosion rates.

Electrochemical impedance spectra were recorded at an open circuit potential, in the frequency range from 100 kHz to  $\sim 10$  mHz and an excitation signal of 5 mV. The ZSimpWin software 3.21 was used to analyze the recorded impedance spectra.

## 2.3. Scanning Electron Microscopy (SEM) and Energy-Dispersive X-Ray Spectroscopy (EDS) Analyses

The morphology of the carbon steel surface products after 72 h of exposure to systems with single components and their mixtures was examined by a scanning electron microscope (SEM) JEOL JSM6510LV, Tokyo, Japan, while the chemical properties of the surface products were determined via energy-dispersive X-ray spectroscopy (EDS). Analyses of the carbon steel were performed after exposure to the system in the presence of individual components separately at concentrations of  $15 \text{ mg dm}^{-3}$   $\text{CeCl}_3$  and  $15 \text{ mg dm}^{-3}$  IOA and in the presence of a mixture of  $15 \text{ mg dm}^{-3}$   $\text{CeCl}_3$  and  $15 \text{ mg dm}^{-3}$  IOA. This combination of the compounds was chosen because most of the test methods showed the highest inhibitory effectiveness at precisely this concentration of the mixture. The samples analyzed were previously sputtered with gold.

## 2.4. Raman Spectroscopy

The Raman spectra of the carbon steel surface corrosion products were obtained using a Bruker Senterra II confocal Raman microscope, Karlsruhe, Germany, with a  $50\times$  long working distance objective. Raman excitation was performed with a Torus single frequency of 532 nm, continuous-wave laser at a laser power of 25 mW and a laser spot diameter of

2–3  $\mu\text{m}$ . Spectra were collected in the 50–4250  $\text{cm}^{-1}$  wavenumber range using a grating with 1200 lines/mm, with an acquisition time of 30 s. The calibration was automatic using SureCAL technology, Bruker, Karlsruhe, Germany. The peak positions were obtained using curve fitting in the Opus software (Base Package).

The samples were analyzed in their original form, without prior preparation, after 72 h of exposure to systems with single components (15  $\text{mg dm}^{-3}$   $\text{CeCl}_3$ ; 15  $\text{mg dm}^{-3}$  IOA) and their mixtures (of 15  $\text{mg dm}^{-3}$   $\text{CeCl}_3$  and 15  $\text{mg dm}^{-3}$  IOA).

### 2.5. Powder X-Ray Diffraction Analysis (PXRD)

The samples of pure carbon steel AISI 1018 and those of carbon steel after 72 h of exposure to the synthetic brine solution saturated with  $\text{CO}_2$  and with the addition of 15  $\text{mg dm}^{-3}$   $\text{CeCl}_3$  were analyzed using the powder method on a Panalytical Empyrean diffractometer, Malvern, UK. Copper radiation ( $K\alpha$  1.541874  $\text{\AA}$ ) was used for the analysis with the following recording conditions:  $U = 45$  kV,  $I = 40$  mA, scan area  $3\text{--}70^\circ 2\Theta$ , step height  $0.0131^\circ$ , scan rate  $0.041683^\circ/\text{s}$ , primary beam divergence  $1/2^\circ$  and PIXcel3D-Medipix3  $1 \times 1$  line detector. Recorded diffractograms were interpreted using the High Score Plus 4.9 (2020) computer program, which uses the PDF-2 database.

## 3. Results and Discussion

### 3.1. Mass Loss Measurement Method

The results of tests using the mass loss method are shown in Table 1 (values of corrosion rates,  $v_{corr}$ , inhibitor effectiveness,  $IE$ , for the uninhibited system and for systems in the presence of individual compounds and their mixtures at different concentrations,  $\gamma$ , and the synergistic parameter,  $S$ ).

**Table 1.** Results obtained using the mass loss method.

System	$\gamma$ ( $\text{mg L}^{-1}$ )	$v_{corr}$ ( $\text{mm year}^{-1}$ )	$IE$ (%)	$S$
Synthetic brine solution	0	1.57	/	/
IOA	5	1.02	$35.03 \pm 0.02$	/
	10	0.58	$63.06 \pm 0.51$	
	15	0.49	$68.79 \pm 0.49$	
	20	0.17	$89.17 \pm 0.92$	
$\text{CeCl}_3$	5	0.53	$66.24 \pm 0.03$	/
	10	0.52	$66.88 \pm 0.15$	
	15	0.53	$66.24 \pm 0.26$	
	20	0.56	$64.33 \pm 0.18$	
$\text{CeCl}_3 + \text{IOA}$	5 + 5	0.29	$81.53 \pm 0.90$	1.17
	5 + 10	0.22	$85.99 \pm 0.94$	0.87
	5 + 15	0.26	$83.43 \pm 0.88$	0.62
	5 + 20	0.14	$91.08 \pm 1.02$	0.40
$\text{CeCl}_3 + \text{IOA}$	10 + 5	0.13	$91.72 \pm 1.12$	2.60
	10 + 10	0.14	$91.08 \pm 0.98$	1.37
	10 + 15	0.13	$91.72 \pm 1.04$	1.27
	10 + 20	0.12	$92.36 \pm 1.22$	0.47
$\text{CeCl}_3 + \text{IOA}$	15 + 5	0.11	$92.99 \pm 1.15$	3.13
	15 + 10	0.08	$94.90 \pm 1.45$	2.45
	15 + 15	0.05	$96.82 \pm 1.86$	2.76
	15 + 20	0.06	$96.18 \pm 1.88$	1.15

The corrosion rate,  $v_{corr}$ , was calculated according to Equation (1):

$$v_{corr} (\text{mm year}^{-1}) = \frac{(m_1 - m_2)}{t\rho A} \quad (1)$$

where  $m_1$  and  $m_2$  are the average mass of samples before and after exposure, respectively;  $A$  is the surface of the carbon steel exposed to the electrolyte;  $t$  is the exposure time, and  $\rho$  is the iron density.

The effectiveness of the inhibitor was calculated from the corrosion rates according to Equation (2):

$$IE (\%) = \left( \frac{v_{corr}^0 - v_{corr}^{inh}}{v_{corr}^0} \right) \times 100 \quad (2)$$

where  $v_{corr}^0$  is the corrosion rate of carbon steel in the system without inhibitor, and  $v_{corr}^{inh}$  is the corrosion rate of carbon steel in the system with individual inhibitor or in the presence of individual inhibitors' mixtures.

The measured mass loss, i.e., the calculated corrosion rate of carbon steel in a chloride-carbonate solution saturated with  $\text{CO}_2$  at  $60^\circ\text{C}$  is  $v_{corr}^{inh} = 1.57 \text{ mm year}^{-1}$ , is in accordance with literature data [47].

The corrosion rate of carbon steel in the presence of cerium(III) chloride is lower (from  $0.52 \text{ mm year}^{-1}$  to  $0.56 \text{ mm year}^{-1}$ ) compared to the uninhibited system ( $1.57 \text{ mm year}^{-1}$ ); however, the corrosion rates and inhibitor effectiveness do not change significantly with increasing  $\text{CeCl}_3$  concentration ( $v_{corr}^{inh}$  from  $0.52 \text{ mm year}^{-1}$  to  $0.56 \text{ mm year}^{-1}$ , i.e.,  $IE$  from 64.24% to 66.88%). The lowest corrosion rate of carbon steel, i.e., the highest effectiveness with the addition of  $\text{CeCl}_3$ , was achieved at a concentration of  $10 \text{ mg/L}$  ( $v_{corr} = 0.52 \text{ mm year}^{-1}$ ,  $IE = 66.88 \pm 0.15\%$ ).

The system in the presence of an imidazoline-based oleic acid inhibitor showed a decrease in the corrosion rate (from  $1.02 \text{ mm year}^{-1}$  to  $0.17 \text{ mm year}^{-1}$ ) and an increase in effectiveness (from 35.03% to 89.17%) with an increase in the concentration of the inhibitor (from  $5 \text{ mg dm}^{-3}$  to  $20 \text{ mg dm}^{-3}$ ). The highest inhibitory efficiency,  $IE = 89.17\%$ , was achieved via IOA at a concentration of  $20 \text{ mg/L}$ .

The synergistic effect of the mixture of two compounds, IOA and  $\text{CeCl}_3$ , as corrosion inhibitors is expressed through a synergistic parameter,  $S$ , which is determined according to Equation (3) [48,49]:

$$S = \frac{1 - IE_{IOA} - IE_{\text{CeCl}_3} + IE_{IOA} \cdot IE_{\text{CeCl}_3}}{1 - IE_{IOA + \text{CeCl}_3}} \quad (3)$$

where  $IE_{IOA}$  and  $IE_{\text{CeCl}_3}$  are the inhibition efficiencies of individual compounds, respectively, while  $IE_{IOA + \text{CeCl}_3}$  is the inhibition efficiency of a mixture of IOA and  $\text{CeCl}_3$ . Values of the synergistic parameter greater than one indicate a synergistic effect of the compounds, while values less than one indicate their antagonistic action [49,50].

Mixtures of compounds IOA and  $\text{CeCl}_3$ , in most of combinations, show synergistic action ( $S > 1$ ) and higher inhibitory effectiveness (from 81.53% to 96.82%) compared to individual components ( $IE$  is from 64.24% to 66.88% for  $\text{CeCl}_3$  and from 35.03% to 89.17% for IOA). The highest inhibitory efficiency,  $IE = 96.82\%$ , was achieved at a mixture concentration of  $15 \text{ mg/dm}^3$   $\text{CeCl}_3$  and  $15 \text{ mg/dm}^3$  IOA.

### 3.2. Results of Electrochemical Measurements

#### 3.2.1. Linear Polarization in a Narrow Range of Potential, $E_{corr} \pm 10 \text{ mV}$

Figure 3 shows the values of polarization resistances,  $R_p$ , with relative standard deviation (less than 5%) determined from the recorded linear polarization curves in a narrow

potential range,  $E_{corr} \pm 10$  mV, for different concentrations of individual components ( $\text{CeCl}_3$  and IOA) and their mixtures after 24 h of exposure to tested electrolyte.

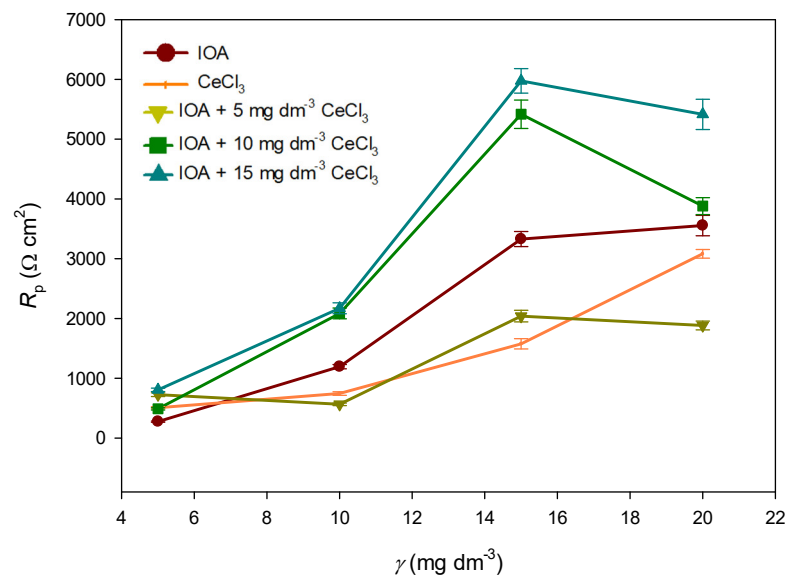


**Figure 3.** Polarization resistance values,  $R_p$ , with relative standard deviation, determined from recorded linear polarization curves in a narrow potential range,  $E_{corr} \pm 10$  mV, for various concentrations of individual components ( $\text{CeCl}_3$  and IOA) and their mixtures.

The values of electrochemical kinetic parameters ( $j_{corr}$ —corrosion current density,  $v_{corr}$ —corrosion rate,  $R_p$ —polarization resistance,  $IE$ —inhibitory efficiency and  $S$ —synergistic parameter) determined from linear polarization curves and recorded on the AISI 1018 carbon steel in a narrow potential range,  $E_{corr} \pm 10$  mV, after 24 h exposure to the tested electrolyte, are shown in Table 2.

In all tested systems, in the presence of individual components,  $\text{CeCl}_3$  and IOA as well as their mixtures, a shift in corrosion potentials in the positive direction, an increase in polarization resistance values and a decrease in corrosion rates compared to the blank system were observed. The efficacies of the tested compounds as corrosion inhibitors, individually and in their mixture, were calculated from the corrosion rate values according to Equation (2). The synergistic effect of each compound's mixture was calculated according to Equation (3).

In the case of IOA, an increase in polarization resistance, from  $275.1 \Omega \text{ cm}^{-2}$  to  $3555.1 \Omega \text{ cm}^{-2}$ , with an increase in concentrations from  $5 \text{ mg dm}^{-3}$  to  $20 \text{ mg dm}^{-3}$  of IOA is observed. The corrosion rate decreases from  $1.115 \text{ mm year}^{-1}$  to  $0.077 \text{ mm year}^{-1}$ , and the effectiveness of IOA as a corrosion inhibitor increases from 11.8% to 92.89%. IOA achieved its highest effectiveness, 92.89%, at a concentration of  $20 \text{ mg dm}^{-3}$ .

The values of polarization resistances,  $R_p$ , for  $\text{CeCl}_3$  show an increase (from  $508.4 \Omega \text{ cm}^{-2}$  to  $3082.9 \Omega \text{ cm}^{-2}$ ) with an increasing concentration (from  $5 \text{ mg dm}^{-3}$  to  $20 \text{ mg dm}^{-3}$ ). The corrosion rates range from  $0.232 \text{ mm year}^{-1}$  to  $0.055 \text{ mm year}^{-1}$ , and the effectiveness of  $\text{CeCl}_3$  as a corrosion inhibitor increases from 81.66% to 95.65%. In the system with  $\text{CeCl}_3$  as a corrosion inhibitor, the highest efficiency, 95.65%, was achieved at the highest concentration of the compound,  $20 \text{ mg dm}^{-3}$ . Compared to the action of IOA alone,  $\text{CeCl}_3$  alone shows greater effectiveness in protecting AISI 1018 carbon steel from corrosion under the tested conditions.

**Table 2.** Electrochemical kinetic parameters determined from linear polarization curves and recorded on the AISI 1018 carbon steel after 24 h exposure to the tested electrolyte.

System	$\gamma$ (mg dm <sup>-3</sup> )	$E_{corr}$ (mV)	$j_{corr}$ ( $\mu$ A cm <sup>-2</sup> )	$R_p$ ( $\Omega$ cm <sup>-2</sup> )	$v_{corr}$ (mm year <sup>-1</sup> )	IE (%)	S
SBS	0	-718	109.0	252.9	1.265	/	/
IOA	5	-709	98.86	275.1	1.115	11.86 ± 0.04	/
	10	-672	24.28	1195.2	0.282	77.71 ± 0.38	
	15	-645	8.23	3329.8	0.096	92.41 ± 1.17	
	20	-644	6.34	3555.1	0.077	92.89 ± 0.95	
CeCl <sub>3</sub>	5	-685	18.00	508.4	0.232	81.66 ± 0.79	/
	10	-679	15.78	745.9	0.183	85.53 ± 0.53	
	15	-690	10.10	1577.2	0.117	90.75 ± 1.32	
	20	-696	4.76	3082.9	0.055	95.65 ± 0.71	
CeCl <sub>3</sub> + IOA	5 + 5	-662	12.40	727.1	0.144	88.62 ± 0.57	1.42
	5 + 10	-675	17.78	565.9	0.206	83.72 ± 1.31	0.16
	5 + 15	-657	7.33	2040.9	0.085	93.28 ± 1.05	0.13
	5 + 20	-656	7.10	1883.1	0.082	93.52 ± 1.30	0.04
CeCl <sub>3</sub> + IOA	10 + 5	-669	22.76	490.1	0.264	79.13 ± 1.44	0.61
	10 + 10	-639	7.37	2085.1	0.085	93.28 ± 1.99	0.48
	10 + 15	-636	3.17	5417.4	0.037	97.08 ± 1.43	0.24
	10 + 20	-642	3.89	3880.9	0.045	96.44 ± 0.93	0.03
CeCl <sub>3</sub> + IOA	15 + 5	-658	9.29	807.4	0.108	91.46 ± 1.35	0.95
	15 + 10	-648	4.73	2171.5	0.055	95.65 ± 2.03	0.47
	15 + 15	-634	2.24	5975.3	0.026	97.94 ± 0.45	0.53
	15 + 20	-635	3.40	5415.5	0.039	96.92 ± 0.28	0.06

Mixtures of 5 mg dm<sup>-3</sup> CeCl<sub>3</sub> and IOA (from 5 mg dm<sup>-3</sup> to 20 mg dm<sup>-3</sup>) do not show an increase in polarization resistance compared to the individual components. However, at higher concentrations of CeCl<sub>3</sub> (10 mg dm<sup>-3</sup> and 15 mg dm<sup>-3</sup>) in mixtures with IOA (5 mg dm<sup>-3</sup>, 10 mg dm<sup>-3</sup>, 15 mg dm<sup>-3</sup> and 20 mg dm<sup>-3</sup>), an increase in polarization resistances is observed compared to the individual components. In mixtures of 15 mg dm<sup>-3</sup> CeCl<sub>3</sub> added to IOA, the highest values of polarization resistance were achieved. Tests at the highest concentrations of the tested mixtures (20 mg dm<sup>-3</sup> IOA in a mixture with 5 mg dm<sup>-3</sup>, 10 mg dm<sup>-3</sup> and 15 mg dm<sup>-3</sup> CeCl<sub>3</sub>) show a decrease in resistance compared to the values of polarization resistances achieved at previous lower concentrations. A possible explanation is that for organic compounds, which IOA is, a critical micellar concentration has been reached [51]. The lowest corrosion rate, 0.026 mm year<sup>-1</sup>, and the highest inhibitory efficacy, 97.94%, were achieved in the presence of a mixture of 15 mg dm<sup>-3</sup> CeCl<sub>3</sub> and 15 mg dm<sup>-3</sup> IOA. Although most combinations of CeCl<sub>3</sub> and IOA mixtures show better performance in corrosion protection of AISI 1018 carbon steel under the tested conditions, compared to the individual components, a synergistic effect ( $S > 1$ ) was demonstrated only for the 5 mg dm<sup>-3</sup> CeCl<sub>3</sub> and 5 mg dm<sup>-3</sup> IOA combination.

### 3.2.2. Potentiodynamic Polarization with Tafel Extrapolation

Polarization curves recorded on carbon steel AISI 1018 in a chloride-carbonate solution saturated with CO<sub>2</sub> at 60 °C without the addition of inhibitors, in the presence of individual components and their mixtures, are shown in Figures 4 and 5.

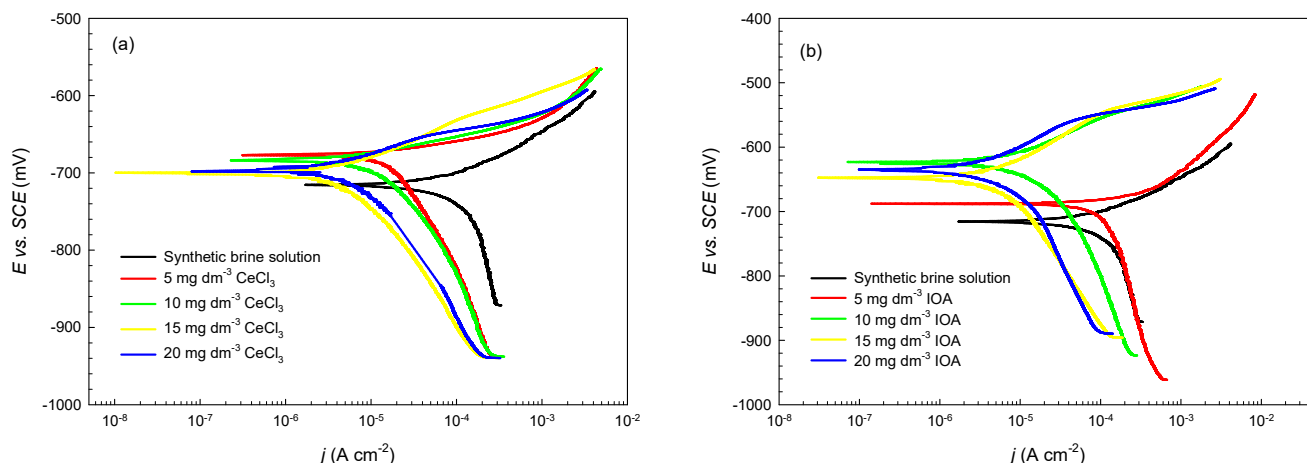


**Figure 4.** Polarization curves recorded on carbon steel AISI 1018 in a chloride–carbonate solution saturated with CO<sub>2</sub> at 60 °C without the addition of inhibitors and in the presence of different concentrations of individual components. (a) CeCl<sub>3</sub> and (b) IOA after 24 h of exposure to the tested electrolyte.

Electrochemical kinetic parameters ( $j_{corr}$ —corrosion current density,  $v_{corr}$ —corrosion rate,  $-\beta_c$  and  $\beta_a$ —cathodic and anodic Tafel slope, respectively,  $IE$ —inhibitory efficiency and  $S$ —synergistic parameter) determined from the polarization curves are summarized in Table 3. The inhibitory efficacies of individual compounds and their mixtures were calculated according to Equation (2), and the synergistic effects of mixtures of compounds were calculated according to Equation (3).

**Table 3.** Electrochemical kinetic parameters determined from the potentiodynamic polarization curves recorded in a potential range of  $E_{corr} \pm 250$  mV relative to the open circuit potential.

System	$\gamma$ (mg dm <sup>-3</sup> )	$E_{corr}$ (mV)	$j_{corr}$ ( $\mu$ A cm <sup>-2</sup> )	$-\beta_c$ (mV dec <sup>-1</sup> )	$\beta_a$ (mV dec <sup>-1</sup> )	$v_{corr}$ (mm year <sup>-1</sup> )	$IE$ (%)	$S$
SBS	0	-713	124.6	410.69	75.01	1.446	/	/
IOA	5	-689	117.0	406.04	68.30	1.358	6.09 ± 0.01	/
	10	-623	15.75	229.49	94.09	0.183	87.34 ± 0.25	
	15	-625	6.72	200.76	91.94	0.078	94.61 ± 0.95	
	20	-582	11.42	152.81	91.62	0.133	90.80 ± 0.87	
CeCl <sub>3</sub>	5	-677	17.87	211.92	23.37	0.207	85.68 ± 0.56	/
	10	-684	14.55	171.32	32.15	0.169	88.31 ± 0.68	
	15	-700	4.67	144.11	49.16	0.054	96.27 ± 0.94	
	20	-694	4.76	117.50	47.30	0.055	96.19 ± 1.03	
CeCl <sub>3</sub> + IOA	5 + 5	-641	15.62	133.12	24.57	0.181	87.48 ± 0.75	1.07
	5 + 10	-658	13.78	112.01	29.18	0.159	89.00 ± 0.67	0.14
	5 + 15	-650	3.54	83.68	58.37	0.041	97.17 ± 1.24	0.07
	5 + 20	-654	3.54	78.13	50.71	0.041	97.17 ± 1.35	0.12
CeCl <sub>3</sub> + IOA	10 + 5	-660	29.91	245.85	28.64	0.347	76.00 ± 0.35	0.46
	10 + 10	-625	5.08	76.05	65.99	0.059	95.91 ± 0.77	0.36
	10 + 15	-626	3.70	96.94	66.75	0.043	97.03 ± 0.69	0.36
	10 + 20	-625	3.70	92.44	78.31	0.043	97.03 ± 0.73	0.36
CeCl <sub>3</sub> + IOA	15 + 5	-639	6.87	77.62	22.18	0.080	94.47 ± 1.02	0.63
	15 + 10	-630	5.83	101.39	30.79	0.067	95.37 ± 1.11	0.10
	15 + 15	-625	2.74	63.49	59.50	0.032	97.78 ± 0.78	0.09
	15 + 20	-629	3.21	84.60	58.80	0.037	97.44 ± 0.25	0.13

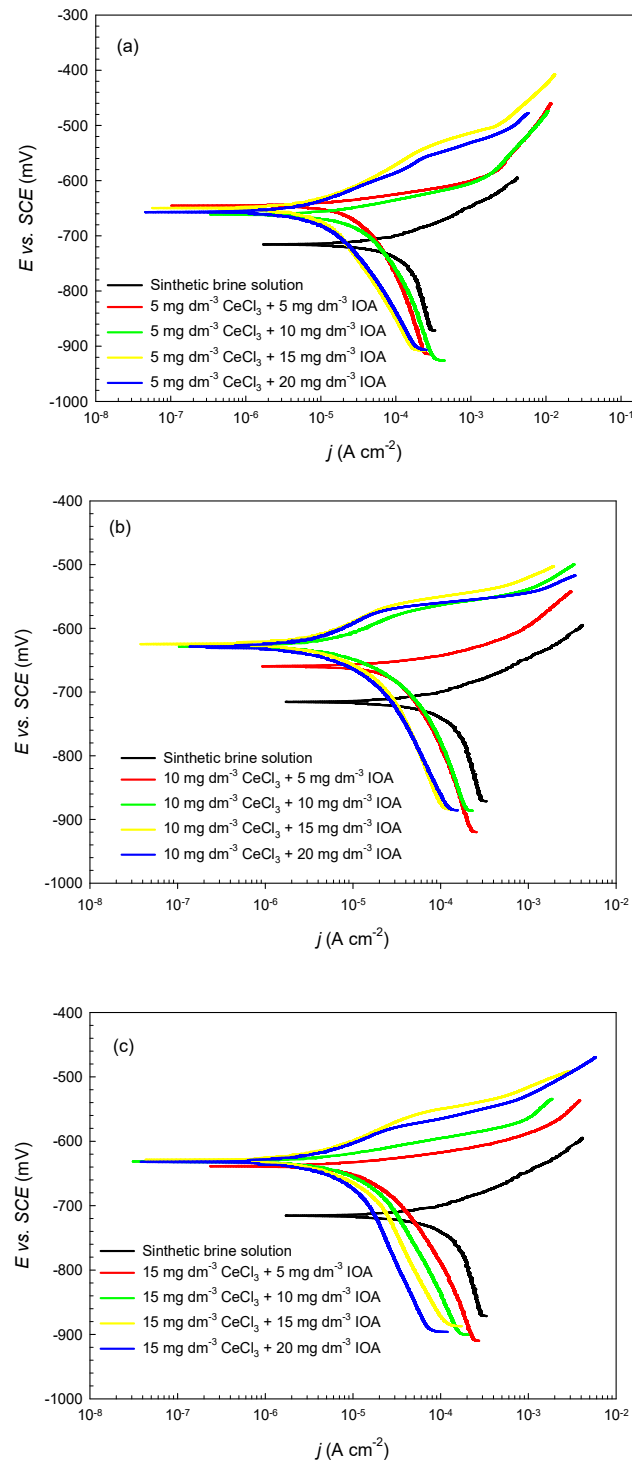
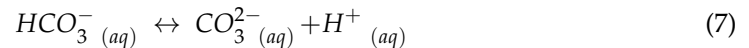
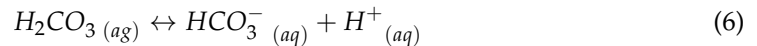
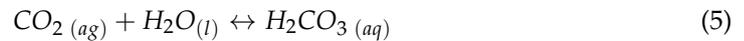


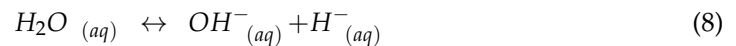
**Figure 5.** Polarization curves recorded on carbon steel AISI 1018 in a chloride–carbonate solution saturated with  $\text{CO}_2$  after 24 h of exposure to the tested electrolyte at  $60^\circ\text{C}$  without the addition of inhibitors and in the presence of different compounds' mixtures: (a)  $5\text{ mg dm}^{-3}$   $\text{CeCl}_3$  and different concentrations of IOA, (b)  $10\text{ mg dm}^{-3}$   $\text{CeCl}_3$  and different concentrations of IOA and (c)  $15\text{ mg dm}^{-3}$   $\text{CeCl}_3$  and different concentrations of IOA.

The mechanism of  $\text{CO}_2$  carbon steel corrosion has been a controversial subject for decades. The system is very complex, involving many chemically and electrochemically active species in an acidic  $\text{CO}_2/\text{H}_2\text{O}$  system.  $\text{CO}_2$  dissolves in water, which then reacts chemically with water to form a weak carbonic acid,  $\text{H}_2\text{CO}_3$ , which dissociates in two steps. In the first step, it dissociates into a hydrogen ion,  $\text{H}^+$ , and a bicarbonate ion,  $\text{HCO}_3^-$ ,

which in the second step, dissociates into a hydrogen ion,  $H^+$ , and a carbonate ion,  $CO_3^{2-}$ , according to the following reactions:



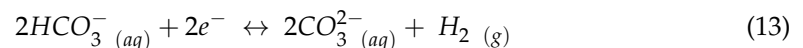
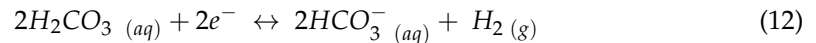
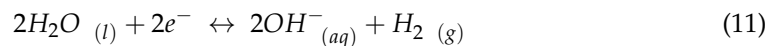
Water as a solvent can dissociate according to the following reaction:



Under the tested conditions, the anodic corrosion reaction is the oxidation of iron from steel according to the following reaction:



Cathodic reactions of  $CO_2$  corrosion involve the reduction of the hydrogen ions,  $H^+$ , either directly or via other weak acids present in the system ( $H_2CO_3$ ,  $HCO_3^-$ ,  $H_2O$ ), according to the following reactions [52]:



It was found that under the test conditions analogous to those in this work, carbonic acid affects the limiting cathodic current but has no effect on the charge transfer current. The charge transfer current depends only on pH, indicating that hydrogen ion reduction is the main cathodic reaction (this mechanism is called the "buffering effect") according to Reaction 10. The direct reduction of carbonic acid is insignificant compared to the reduction of hydrogen ions [52,53].

The polarization curve recorded on carbon steel after 24 h of exposure to the inhibitor-free system (black curve in Figures 4 and 5) shows cathodic corrosion currents partly influenced by mass transfer, while the anodic polarization curves show a linear dependence of current and potential, indicating a region of active dissolution, i.e., iron oxidation [54].

In the presence of IOA, an inhibitory effect on the cathodic and anodic process was observed, i.e., a shift in the cathodic and anodic polarization curves towards lower values of the corrosion current density and thus lower corrosion rates. Such an inhibitory action is more pronounced with an increase in the concentration of IOA, which is evident from the polarization curves (Figure 4) as well as the kinetic parameters contained in Table 3. The slopes of the anodic Tafel lines in the presence of IOA change slightly ( $68.30 \text{ mV dec}^{-1}$ – $94.09 \text{ mV dec}^{-1}$ ) compared to the value of the slope in the uninhibited solution ( $75.01 \text{ mV dec}^{-1}$ ), which points to the effect of IOA in the way that it adsorbs on the metal surface, blocks the active sites and prevents the anodic reaction from taking place rather than changing the mechanism of the anodic reaction [13,14,51]. The dominant cathodic reduction reaction in the test conditions ( $CO_2$ -saturated brine solution,  $pH \approx 5$ ) is the reduction of hydrogen ions produced via the dissociation of carbonic acid. The slope of

the cathodic Tafel line of the uninhibited system is high ( $410.69 \text{ mV dec}^{-1}$ ) in electrolytes due to the influence of diffusion of  $\text{H}^+$  ions on the cathodic reaction. In the presence of IOA, a decrease in the slope of the cathodic Tafel line ( $406.04 \text{ mV dec}^{-1}$ – $152.81 \text{ mV dec}^{-1}$ ) is observed, but it is still high, indicating the influence of diffusion on the cathodic process [15]. In the presence of IOA, the corrosion potential is shifted towards more positive values (from  $-689 \text{ mV}$  to  $-582 \text{ mV}$ ), which indicates a preference for inhibiting the anodic reaction and is associated with the formation of a protective film [17,51]. At higher concentrations of IOA (from  $10 \text{ mg dm}^{-3}$  to  $20 \text{ mg dm}^{-3}$ ), the corrosion potential shift in the anodic direction is greater than  $85 \text{ mV}$  compared to the system without inhibitors, classifying it as an anodic type of corrosion inhibitor under the tested conditions [18–23,51]. It slows down corrosion by reducing the rate of the anodic metal dissolution process. The values of inhibitory effectiveness, shown in Table 2, increase with the increase in IOA concentration and reach a maximum value of 94.61% at a concentration of  $15 \text{ mg dm}^{-3}$ , which is attributed to the binding of imidazoline molecules to the metal surface. The structure of IOA (Figure 2a) shows the existence of delocalized electrons in the imidazole ring as well as a free electron pair on the nitrogen atoms. The adsorption of IOA on the surface of carbon steel AISI 1018 can be explained in the way that IOA can donate these  $\pi$ -electrons and free electron pairs to the empty d-orbitals of iron [55,56].

The presence of  $\text{CeCl}_3$  causes a shift in the corrosion potential slightly in the positive direction (from  $-677 \text{ mV}$  to  $-699 \text{ mV}$ ) compared to the blank system ( $-713 \text{ mV}$ ). At all tested  $\text{CeCl}_3$  concentrations, a displacement of the cathodic and anodic branches of the polarization curves towards lower corrosion currents is observed. The corrosion current densities (from  $17.87 \text{ } \mu\text{A cm}^{-2}$  to  $4.67 \text{ } \mu\text{A cm}^{-2}$ ) and corrosion rates (from  $0.207 \text{ mm year}^{-1}$  to  $0.054 \text{ mm year}^{-1}$ ) are significantly lower compared to the values recorded for the same concentrations in the presence of IOA (from  $117.0 \text{ } \mu\text{A cm}^{-2}$  to  $6.72 \text{ } \mu\text{A cm}^{-2}$  and from  $1.358 \text{ mm year}^{-1}$  to  $0.078 \text{ mm year}^{-1}$ ) and the blank system ( $124.6 \text{ } \mu\text{A cm}^{-2}$ ,  $1.446 \text{ mm year}^{-1}$ ).  $\text{CeCl}_3$  significantly reduced the slope of the cathodic Tafel line (from  $211.92 \text{ mV dec}^{-1}$  to  $117.50 \text{ mV dec}^{-1}$ ) compared to the blank system ( $410.69 \text{ mV year}^{-1}$ ), as shown in Figure 4 and Table 3, indicating the effect of  $\text{CeCl}_3$  on the cathodic reaction. The sustained high slopes of the cathodic Tafel lines indicate the influence of diffusion on the cathodic reaction [15]. The slopes of the anodic Tafel line are significantly lower (from  $47.30 \text{ mV dec}^{-1}$  to  $23.37 \text{ mV dec}^{-1}$ ) compared to the uninhibited system ( $75.01 \text{ mV dec}^{-1}$ ), indicating an influence of  $\text{CeCl}_3$  on the anodic corrosion reaction of ferrous oxidation. The effectiveness of  $\text{CeCl}_3$  in protecting AISI 1018 carbon steel from corrosion increases with increasing concentration (from  $5 \text{ mg dm}^{-3}$  to  $15 \text{ mg dm}^{-3}$ ). However, a deviation from this trend was observed at the highest tested concentration ( $20 \text{ mg dm}^{-3}$ ), where a slight increase in the corrosion rate and a decrease in inhibitory efficiency, compared to values at  $15 \text{ mg dm}^{-3}$   $\text{CeCl}_3$ , were observed, which can be explained by the increase in chloride concentration when adding a higher concentration of  $\text{CeCl}_3$  [33,57–59].  $\text{CeCl}_3$  showed the behavior of a mixed corrosion inhibitor with a predominant influence on the anodic process. The highest inhibitory efficiency, 96.27%, was shown by  $\text{CeCl}_3$  at a concentration of  $15 \text{ mg dm}^{-3}$ , which potentially can be attributed to the formation of cerium carbonate under the tested conditions [57].

The corrosion potential values for all tested compound mixtures show a shift in the anodic direction compared to the blank system ( $-713 \text{ mV}$ ). The range of corrosion potential for the compound mixtures ranges from  $-660 \text{ mV}$  to  $-625 \text{ mV}$ ; in some mixtures, only a negligible increase in potential (slightly above  $85 \text{ mV}$ ) compared to the uninhibited system was observed. The values of corrosion currents and corrosion rates are very low in the presence of the compounds' mixtures, which are already at low concentrations of compounds. The slopes of the cathodic and anodic Tafel lines in the presence of the

mixtures of compounds are comparable or lower to those determined in the systems with the individual components, indicating the effect of the mixtures of compounds on the cathodic and anodic corrosion reactions. The mixture of tested compounds blocks the metal surface and reduces the areas available for cathodic and anodic reactions to occur [57]. From the above results, the mixture of  $\text{CeCl}_3$  and IOA compounds showed the activity of a mixed corrosion inhibitor with a significant effect on the anodic reaction of iron oxidation. The highest inhibitory efficiency, 97.78%, was shown by the mixture composed of  $15 \text{ mg dm}^{-3}$   $\text{CeCl}_3$  and  $15 \text{ mg dm}^{-3}$  IOA. Most of the mixtures of compounds did not show synergistic action, since as individual components, they achieved high inhibitory efficiency. Nonetheless, an enhanced corrosion protection effect was certainly noted compared to individual compounds. Synergistic action ( $S = 1.07$ ) was proven only for the combination of the lowest concentrations of compounds:  $5 \text{ mg dm}^{-3}$   $\text{CeCl}_3$  and  $5 \text{ mg dm}^{-3}$  IOA, with a corresponding effectiveness of 87.48%.

At higher concentrations of individual components and their mixtures, an increase in the slope of the anodic polarization curves, immediately after  $E_{corr}$ , is observed (seen in Figures 4 and 5), and it is attributed to the adsorption of the inhibitor onto the steel surface. This is followed by an abrupt increase in the corrosion current density with increasing potential, indicating the desorption of the inhibitor. The surface coverage of the adsorbed inhibitor usually decreases with increasing potential because the adsorbed compounds become unstable at high polarization potentials [60].

### 3.2.3. Electrochemical Impedance Spectroscopy (EIS)

The phenomena at the electrolyte/carbon steel surface interface were investigated using electrochemical impedance spectroscopy. Nyquist and Bode impedance spectra recorded on carbon steel AISI 1018 in a chloride–carbonate solution saturated with and without  $\text{CO}_2$  and in the presence of individual components,  $\text{CeCl}_3$  and IOA, are shown in Figure 6, while spectra recorded in the presence of mixtures of compounds are shown in Figures 7–9.

The recorded impedance spectra for all tested systems are matched to the equivalent electrical circuit models, as shown in Figure 10. EIS parameters determined by that matching are presented in Table 4.

Based on the presented Nyquist and Bode diagrams, the points represent the experimental values, while the lines represent the values of the assumed theoretical model of the electrical equivalent circuit. The results of matching experimental and theoretical values show a very good agreement, with a deviation of less than 5% for each spectrum. Selected theoretical models of electrical circuits, according to the literature, are used to interpret impedance spectra recorded under similar conditions as those listed in this paper [52,61,62].

Three electrical equivalent circuits were used in the analysis of impedance spectra. The circuit shown in Figure 10a was used in the analysis of spectra recorded in the blank system, while the circuits shown in Figure 10b,c were used for spectra recorded in systems containing individual components of  $\text{CeCl}_3$ , IOA and in the presence of their mixtures. The circuit shown in Figure 10c was used in the analysis of the recorded spectra exhibiting an inductive loop, and the circuit shown in Figure 10b was used in the absence of an inductive loop.

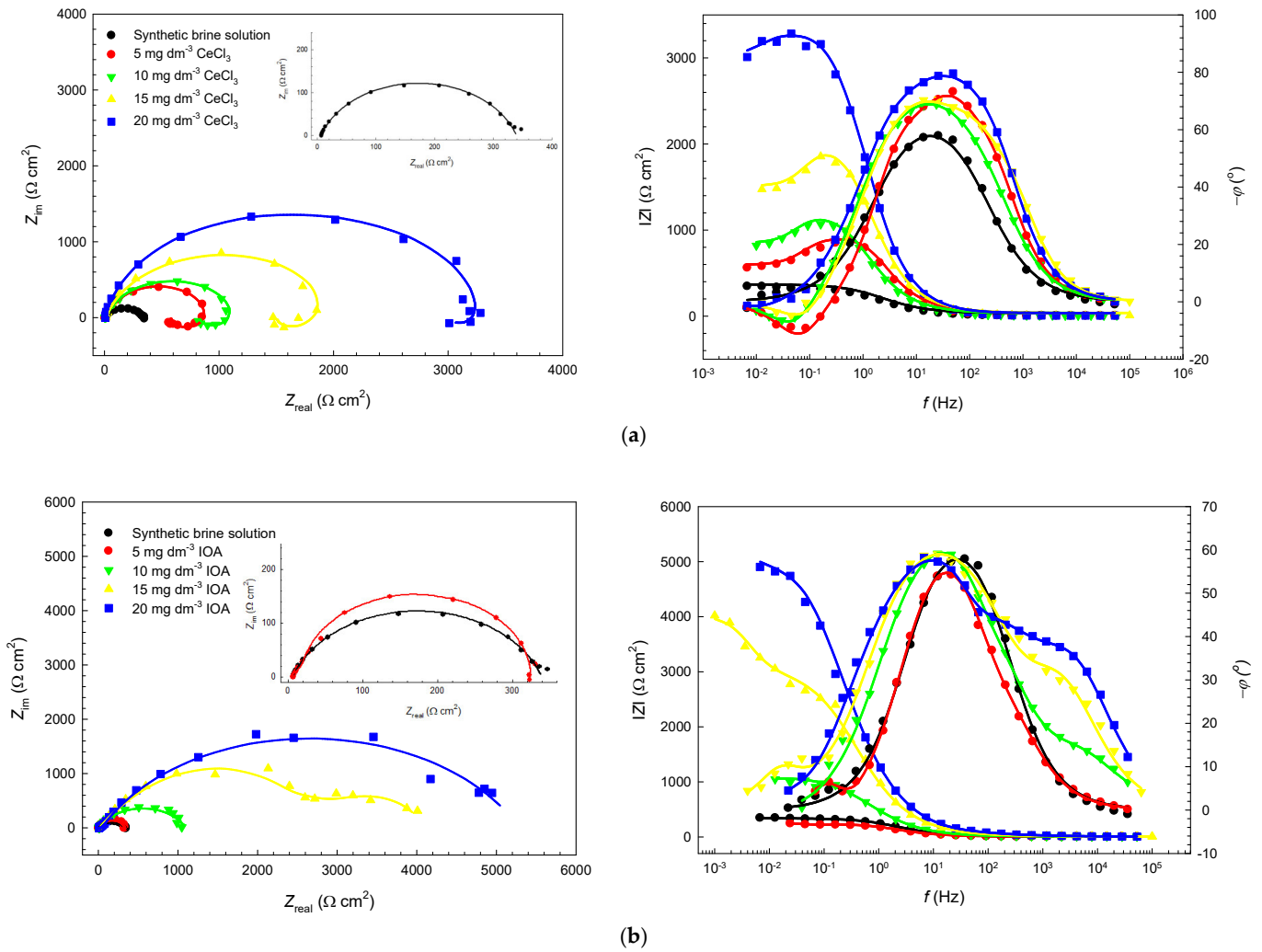


**Figure 6.** Nyquist and Bode diagrams of impedance spectra recorded on AISI 1018 carbon steel in chloride–carbonate solution saturated with and without CO<sub>2</sub> and in the presence of different concentrations of individual compounds, CeCl<sub>3</sub> (a) and IOA (b) after 24 h of exposure to the tested electrolyte at 60 °C.

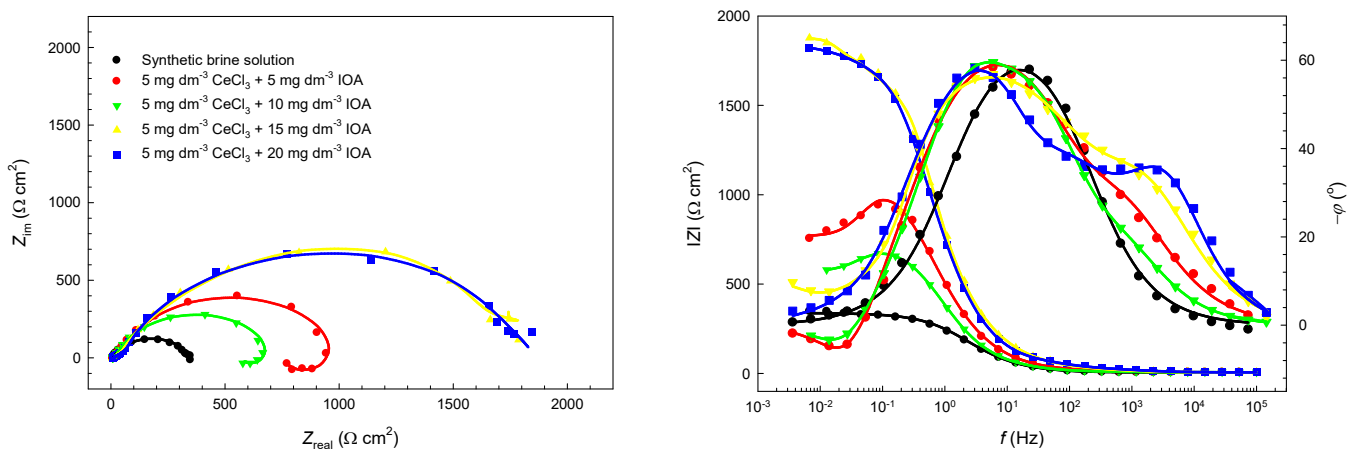


**Figure 7.** Nyquist and Bode diagrams of impedance spectra recorded on AISI 1018 carbon steel in chloride–carbonate solution saturated with and without CO<sub>2</sub> and in the presence of mixtures of IOA (in concentrations of 5 mg dm<sup>-3</sup>, 10 mg dm<sup>-3</sup>, 15 mg dm<sup>-3</sup> and 20 mg dm<sup>-3</sup>) and 5 mg dm<sup>-3</sup> of CeCl<sub>3</sub>.

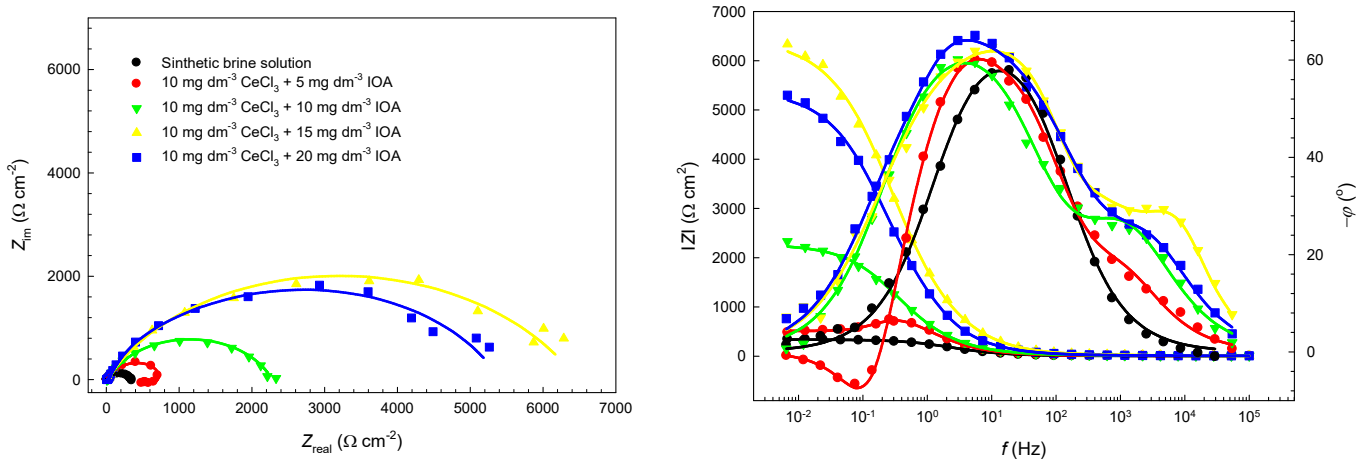


**Figure 8.** Nyquist and Bode diagrams of impedance spectra recorded on AISI 1018 carbon steel in chloride–carbonate solution saturated with and without CO<sub>2</sub> and in the presence of mixtures of IOA (in concentrations of 5 mg dm<sup>-3</sup>, 10 mg dm<sup>-3</sup>, 15 mg dm<sup>-3</sup> and 20 mg dm<sup>-3</sup>) and 10 mg dm<sup>-3</sup> of CeCl<sub>3</sub>.

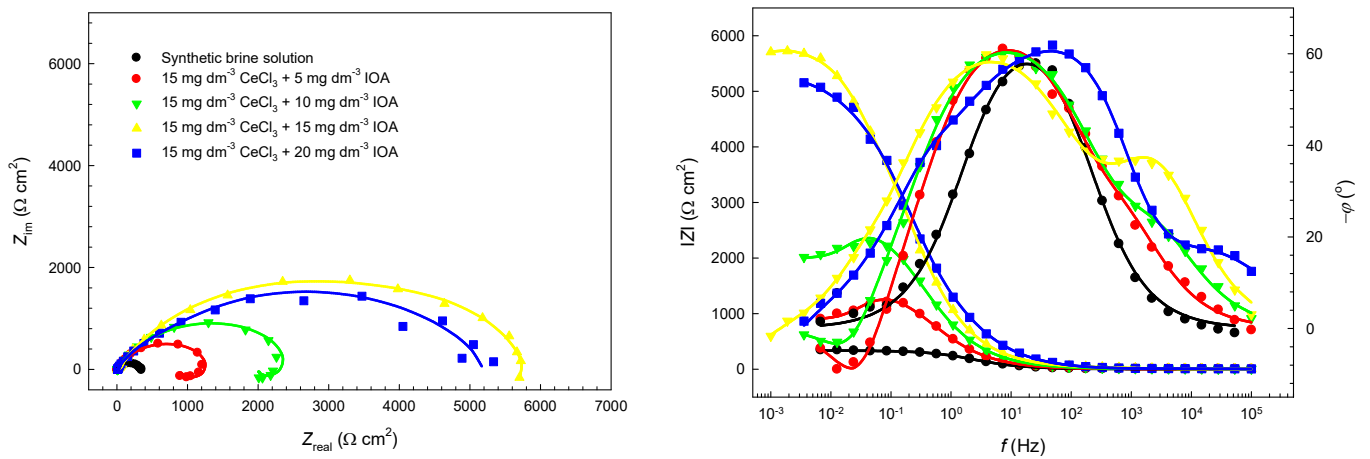


**Figure 9.** Nyquist and Bode diagrams of impedance spectra recorded on AISI 1018 carbon steel in chloride–carbonate solution saturated with and without CO<sub>2</sub> and in the presence of mixtures of IOA (in concentrations of 5 mg dm<sup>-3</sup>, 10 mg dm<sup>-3</sup>, 15 mg dm<sup>-3</sup> and 20 mg dm<sup>-3</sup>) and 15 mg dm<sup>-3</sup> of CeCl<sub>3</sub>.

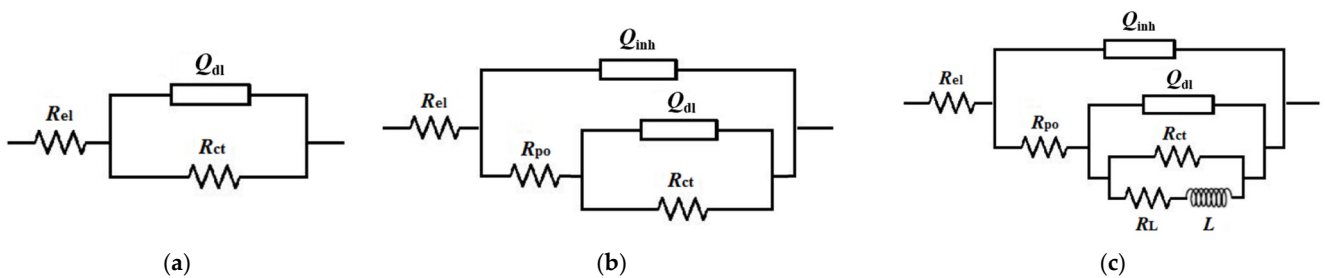


**Figure 10.** Equivalent electrical circuits used for the analysis of the recorded impedance spectra of AISI 1018 carbon steel in (a) a chloride–carbonate solution without inhibitors and (b,c) in the presence of individual components (CeCl<sub>3</sub> and IOA) and their mixtures.

**Table 4.** EIS parameters (with chi-square distribution,  $\chi^2$ ) determined by fitting the recorded impedance spectra in the tested electrolytes with the assumed electrical equivalent circuit model.

System	$\gamma$ (mg L <sup>-1</sup> )	$R_{el}$ ( $\Omega$ cm <sup>-2</sup> )	$Q_{inh}$ ( $\mu S s^n$ )	$R_{po}$ ( $\Omega$ cm <sup>-2</sup> )	$n_{inh}$	$Q_{dl}$ ( $\mu S s^n$ )	$R_{ct}$ ( $\Omega$ cm <sup>-2</sup> )	$n$	$L$ (Henri)	$R_L$ ( $\Omega$ cm <sup>-2</sup> )	$IE$ (%)	$S$	$\chi^2$ ( $\cdot 10^{-4}$ )
SBS	0	6.742	/	/	/	1463.7	332.5	0.806	/	/	/	/	1.02
IOA	5	6.889	395.8	15.54	0.826	244.8	344.3	0.826	/	/	3.43 ± 0.01	/	1.01
	10	6.632	104.9	8.467	0.811	286.4	1086.0	0.779	/	/	69.38 ± 0.64	/	2.74
	15	6.364	287.6	119.7	0.749	167.9	3257.0	0.718	/	/	89.79 ± 0.84	/	4.86
	20	6.101	95.39	92.81	0.822	86.48	5203.0	0.765	/	/	93.61 ± 0.56	/	2.61
CeCl <sub>3</sub>	5	6.593	62.64	102.5	0.892	143.5	783.89	0.968	558.5	330.9	57.58 ± 0.27	/	1.49
	10	6.832	132.4	64.07	0.857	59.81	1159.7	0.794	862.8	327.8	71.33 ± 0.86	/	3.51
	15	6.867	24.77	27.89	0.848	68.70	2035.0	0.908	803.9	314.3	83.66 ± 0.55	/	2.44
	20	6.593	56.05	19.90	0.858	45.06	3677.6	0.947	883.1	310.5	90.96 ± 0.78	/	2.43
CeCl <sub>3</sub> + IOA	5 + 5	6.657	179.7	23.91	0.763	189.2	935.2	0.738	944.9	364.5	64.45 ± 0.06	1.15	2.24
	5 + 10	6.202	169.9	22.63	0.737	172.3	1050.1	0.831	877.5	355.2	68.34 ± 0.35	0.41	4.23
	5 + 15	6.688	38.06	21.98	0.747	168.1	1836.9	0.837	/	/	81.90 ± 0.98	0.24	1.77
	5 + 20	6.776	13.86	22.38	0.763	225.9	1829.3	0.905	/	/	81.82 ± 1.12	0.15	3.69
CeCl <sub>3</sub> + IOA	10 + 5	6.785	91.96	9.78	0.798	191.3	893.2	0.826	952.6	372.1	62.77 ± 0.69	0.74	2.70
	10 + 10	6.620	80.12	24.52	0.748	237.0	2245.1	0.782	/	/	85.19 ± 0.78	0.59	1.48
	10 + 15	6.618	62.67	12.99	0.735	124.6	6539.5	0.788	/	/	94.92 ± 1.29	0.58	2.16
	10 + 20	6.654	37.02	17.35	0.709	153.0	5836.1	0.739	/	/	94.30 ± 1.32	0.32	3.12
CeCl <sub>3</sub> + IOA	15 + 5	6.798	169.0	18.84	0.782	178.4	1424.0	0.776	970.0	354.5	76.65 ± 1.45	0.67	1.53
	15 + 10	6.986	75.95	15.40	0.765	180.9	2711.5	0.747	860.0	228.7	87.74 ± 1.39	0.41	1.17
	15 + 15	6.811	33.61	40.06	0.802	180.3	5831.4	0.722	857.7	209.6	94.30 ± 1.68	0.29	5.07
	15 + 20	6.359	147.8	12.22	0.703	29.32	5435.0	0.785	/	/	93.88 ± 0.29	0.17	1.55

The elements of the chosen electrical equivalent circuits are as follows: electrolyte resistance,  $R_{el}$ , charge transfer resistance,  $R_{ct}$ , pore resistance of the inhibitor film,  $R_{po}$ , inductance,  $L$ , resistance of the inductance,  $R_L$ , constant phase element equivalent to the capacity of the electrochemical double layer,  $Q_{dl}$ , and constant phase element equivalent to the capacity of the inhibitor film,  $Q_{inh}$ . A constant phase element, in the electric equivalent circuit, is used instead of a capacitor because it compensates for surface inhomogeneity, geometric irregularity, roughness, and porosity of the electrode, etc., [62,63].

The impedance of a constant phase element is calculated according to

$$Z = \frac{1}{Q} (j\omega)^{-n} \quad (14)$$

where  $Q$  is the proportionality factor;  $j = \sqrt{-1}$ ,  $\omega = 2\pi f$  and  $n$  are the dispersion coefficients associated with surface inhomogeneity. Depending on the value of the coefficient  $n$ , the constant phase element can be represented by a resistor (for  $n = 0$   $R = Q^{-1}$ ) or a capacitor (for  $n = 1$   $C = Q$ ). The physical meaning of coefficient  $n$  has not been fully clarified [64,65].

The inhibitory efficacy,  $IE$ , of individual compounds, CeCl<sub>3</sub> and IOA, as well as their mixtures was calculated according to the following equation:

$$IE = \frac{R_{ct}^{inh} - R_{ct}^0}{R_{ct}^{inh}} \times 100 \quad (15)$$

where  $R_{ct}^{inh}$  represents the charge transfer resistance of carbon steel for the system in the presence of individual CeCl<sub>3</sub> and IOA compounds and their mixtures, while  $R_{ct}^0$  represents the charge transfer resistance for the uninhibited system.

The Nyquist diagram recorded on AISI 1018 carbon steel in a synthetic brine solution saturated with CO<sub>2</sub> and without an inhibitor shows the existence of one capacitive semicircle, as shown in Figure 6. The Bode diagram shows the existence of a single time constant, which indicates an active corrosion process and the formation of corrosion products that do not possess good protective properties [66]. In the analysis of the recorded impedance spectrum for the uninhibited system, the equivalent circuit shown in Figure 10a was used. For similar test conditions, according to the literature, the same equivalent circuit in the

analysis of the recorded impedance spectra is used, and by matching the recorded spectrum with the assumed model, a very good agreement was achieved ( $\chi^2 = 1.02 \cdot 10^{-4}$ ). Although the recorded polarization curves for the uninhibited system (Figure 4) show the influence of diffusion on the cathodic reaction, it is not observed in the recorded impedance spectrum. Therefore, the application of the model that includes the Warburg element would result in a large error [67]. The high value of the proportionality factor  $Q_{dl} = 1463.7 \mu\text{S s}^n$  is in accordance with the literature data and is consistent with the high value of the double layer capacity in synthetic brine solutions saturated with  $\text{CO}_2$  as a result of the large surface area available for the deposition of corrosion products. This can be explained by the ferrite–pearlite microstructure of AISI 1018 carbon steel, where ferrite preferentially dissolves during active corrosion processes while cementite remains, protruding from the steel surface [62,63,68].

In the presence of  $\text{CeCl}_3$ , compared to the blank system, an increase in the real and imaginary impedance components on the Nyquist diagram (Figure 6) is observed. This increase is in line with the increase in  $\text{CeCl}_3$  concentration, which can be attributed to the formation of a protective film [69]. The recorded spectra show the existence of a small inductive loop in the very-low-frequency range. The inductive loop indicates that the adsorbed inhibitor layer becomes unstable and desorbs from the metal surface, which enhances the relaxation adsorption–desorption processes of the inhibitor. As a result of the destabilization of the adsorbed inhibitory layer, the anodic dissolution of the metal increases [70,71]. In the Bode plots, there is one phase angle peak where the maximum broadens and increases with increasing  $\text{CeCl}_3$  concentration, which can be attributed to the formation of an inhibitor film on the carbon steel surface [66]. The impedance modulus also increases with increasing  $\text{CeCl}_3$  concentration. Since the recorded impedance spectra in the presence of  $\text{CeCl}_3$  show the existence of an inductive loop, the equivalent electrical circuit shown in Figure 10c was used in the analysis. The influence of diffusion, which is visible in the recorded polarization curves in the presence of  $\text{CeCl}_3$ , is not visible in the impedance spectra, and the equivalent circuit with the Warburg element was not used. According to the values in Table 4, the charge transfer resistances,  $R_{ct}$ , in the presence of  $\text{CeCl}_3$  are higher than the charge transfer resistance for the blank system ( $332.5 \Omega \text{ cm}^2$ ), and they increase (from  $783.9 \Omega \text{ cm}^2$  to  $3677.6 \Omega \text{ cm}^2$ ) with increasing  $\text{CeCl}_3$  concentration (from  $5 \text{ mg dm}^{-3}$  to  $20 \text{ mg dm}^{-3}$ ). The values of the constant phase element,  $Q_{dl}$ , show lower values (from  $143.5 \mu\text{S s}^n$  to  $45.06 \mu\text{S s}^n$ ) compared to the uninhibited system ( $1463.7 \mu\text{S s}^n$ ), indicating the adsorption of  $\text{CeCl}_3$  on the steel surface. The inhibitory efficiency, calculated according to Equation (15), increases (from 57.58% to 90.96%) with increasing  $\text{CeCl}_3$  concentration and achieves the highest value, 90.96%, at  $20 \text{ mg dm}^{-3} \text{ CeCl}_3$ .

The presence of IOA in the synthetic brine solution on the recorded Nyquist diagrams (Figure 6) is manifested through the increase in capacitive semicircles with increasing IOA concentration. At concentrations above  $5 \text{ mg dm}^{-3}$  on the Nyquist diagrams, and especially the Bode diagram, in addition to the time constant in the low-frequency range, the appearance of a time constant in the high-frequency region is observed. The maxima of the high-frequency phase angle peaks increase with increasing concentration as do the impedance modules. All the above indicates the formation of an inhibitory film of IOA on the steel surface [39,66]. The electrical equivalent circuit shown in Figure 10b was used in the analysis of the recorded impedance spectra, and a very good agreement was achieved ( $\chi^2 = 1.01 \cdot 10^{-4}$ – $4.86 \cdot 10^{-4}$ ). The analysis results, contained in Table 4, show an increase in charge transfer resistance (from  $344.3 \Omega \text{ cm}^2$  to  $5203.0 \Omega \text{ cm}^2$ ) with increasing IOA concentration (from  $5 \text{ mg dm}^{-3}$  to  $20 \text{ mg dm}^{-3}$ ), which indicates the protective effect of the inhibitor film against carbon steel corrosion under the tested conditions. Lower  $Q_{dl}$  values (from  $286.4 \mu\text{S s}^n$  to  $86.48 \mu\text{S s}^n$ ) compared to the blank system ( $1463.7 \mu\text{S s}^n$ )

indicate the adsorption of IOA onto the carbon steel surface. The decrease in the double layer capacitance, i.e.,  $Q_{dl}$ , can be explained (via the Helmholtz model) by the replacement of water molecules (high dielectric constant) on the steel surface with inhibitor molecules (low dielectric constant). Another explanation is the increase in the double layer thickness due to the adsorption of larger organic inhibitor molecules on the steel surface, which results in a decrease in the double layer capacitance [72,73]. The effectiveness of IOA as a corrosion inhibitor increases with increasing concentration (from 3.43% to 93.61%) and shows the highest effectiveness, 93.6%, at a concentration of  $20 \text{ mg dm}^{-3}$ .

The impedance spectra (Nyquist and Bode plots) recorded for mixtures of  $\text{CeCl}_3$  and IOA compounds are shown in Figures 7–9, while the results of the fitting with equivalent electrical circuits (shown in Figure 10b,c) are contained in Table 4. The recorded impedance spectra in the presence of compound mixtures, in some combinations of concentrations, show the existence of an inductive loop. For them, the best fitting is achieved with the model shown in Figure 10c. For those combinations of compound mixtures, whose spectra do not show the existence of an inductive loop, the best fitting is achieved with the equivalent circuit model shown in Figure 10b. For all tested combinations of  $\text{CeCl}_3$  and IOA mixtures, a single capacitive semicircle is observed in the Nyquist plots in the high- and medium-frequency range, and for some tested mixtures, an inductive loop is observed in the low-frequency range. The irregular shape of the semicircle is an indicator of the impedance frequency dispersion at the interface and a characteristic of the inhomogeneity of the carbon steel surface [74,75]. In the presence of compound mixtures, the Bode plots show the appearance of phase angle peaks in the low- and high-frequency range. The phase angle maxima in the low-frequency range are higher and more extended compared to the blank system, while the phase angle maxima in the high-frequency range increase and shift to the higher frequency range with increasing compound mixture concentrations. All this indicates that the tested compound mixtures form an inhibitory film on the steel surface [39]. The recorded impedance spectra for the compound mixtures are like those for IOA but with a more prominent inhibitory effect, especially with the addition of  $10 \text{ mg dm}^{-3}$  and  $15 \text{ mg dm}^{-3}$   $\text{CeCl}_3$  to IOA. The influence of  $\text{CeCl}_3$  on the improved inhibitory action of IOA is more pronounced when adding  $\text{CeCl}_3$  in higher concentrations, specifically at  $10 \text{ mg dm}^{-3}$  and  $15 \text{ mg dm}^{-3}$ . Table 4. shows that with an increase in the concentration of  $\text{CeCl}_3$  (from  $5 \text{ mg dm}^{-3}$  to  $15 \text{ mg dm}^{-3}$ ) added to IOA (from  $5 \text{ mg dm}^{-3}$  to  $20 \text{ mg dm}^{-3}$ ), high values of charge transfer resistances are achieved (from  $893.2 \Omega \text{ cm}^2$  to  $6539.5 \Omega \text{ cm}^2$ ). The mixture of  $10 \text{ mg dm}^{-3}$   $\text{CeCl}_3$  and  $15 \text{ mg dm}^{-3}$  IOA showed the highest charge transfer resistance,  $6539.5 \Omega \text{ cm}^2$ , and the highest inhibitory efficiency, 94.92%. The  $Q_{dl}$  values in the presence of the compound mixtures are lower than the  $Q_{dl}$  values for the blank system and comparable or in some cases even lower than the  $Q_{dl}$  values for the system in the presence of IOA. Thus, in the presence of the compound mixtures, a protective layer is formed on the surface of the carbon steel that has better protective properties compared to the system in the presence of a single IOA. Although the synergistic effect of the compounds  $\text{CeCl}_3$  and IOA ( $S > 1$ ) was proven only in the case of the lowest concentrations of the compounds,  $5 \text{ mg dm}^{-3}$  and  $5 \text{ mg dm}^{-3}$ , at higher concentrations of  $\text{CeCl}_3$  ( $10 \text{ mg dm}^{-3}$  and  $15 \text{ mg dm}^{-3}$ ), the effect of the compound mixtures in corrosion protection is clearly enhanced. The addition of  $\text{CeCl}_3$  at concentrations of  $10 \text{ mg dm}^{-3}$  and  $15 \text{ mg dm}^{-3}$  to IOA caused higher inhibitory efficacy (from 67.77% to 94.92%) compared to the single IOA (from 3.43% to 93.61%).

### 3.3. Carbon Steel Surface Morphology

Most methods used for testing the effect of  $\text{CeCl}_3$  addition to IOA on inhibitory activity showed the best effect for the mixture of  $15 \text{ mg dm}^{-3}$   $\text{CeCl}_3$  and  $15 \text{ mg dm}^{-3}$

IOA. Therefore, this mixture of compounds was chosen for surface analysis, as well as the concentrations of the individual compounds. Figure 11 shows SEM images of the surfaces of AISI 1018 carbon steel after 72 h of exposure to a CO<sub>2</sub>-saturated brine solution in the presence of individual compounds of 15 mg dm<sup>-3</sup> CeCl<sub>3</sub> (a), 15 mg dm<sup>-3</sup> IOA (b) and their mixtures (c). The corresponding EDS mapping analysis of elements on the carbon steel surface is shown in Figure 12.

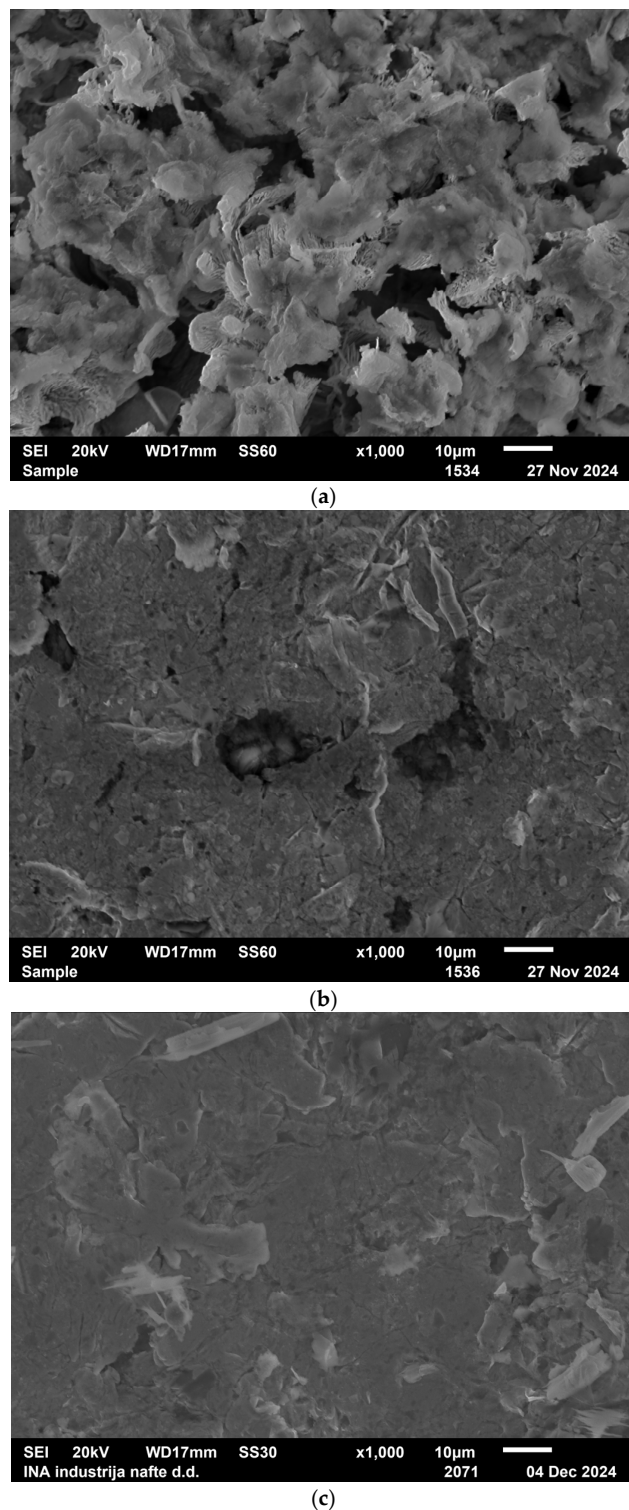


**Figure 11.** SEM images of carbon steel AISI 1018 surfaces after 72 h of exposure to a chloride-carbonate solution saturated with CO<sub>2</sub> in the presence of (a) 15 mg dm<sup>-3</sup> CeCl<sub>3</sub>, (b) 15 mg dm<sup>-3</sup> IOA and (c) the mixture of 15 mg dm<sup>-3</sup> CeCl<sub>3</sub> and 15 mg dm<sup>-3</sup> IOA.

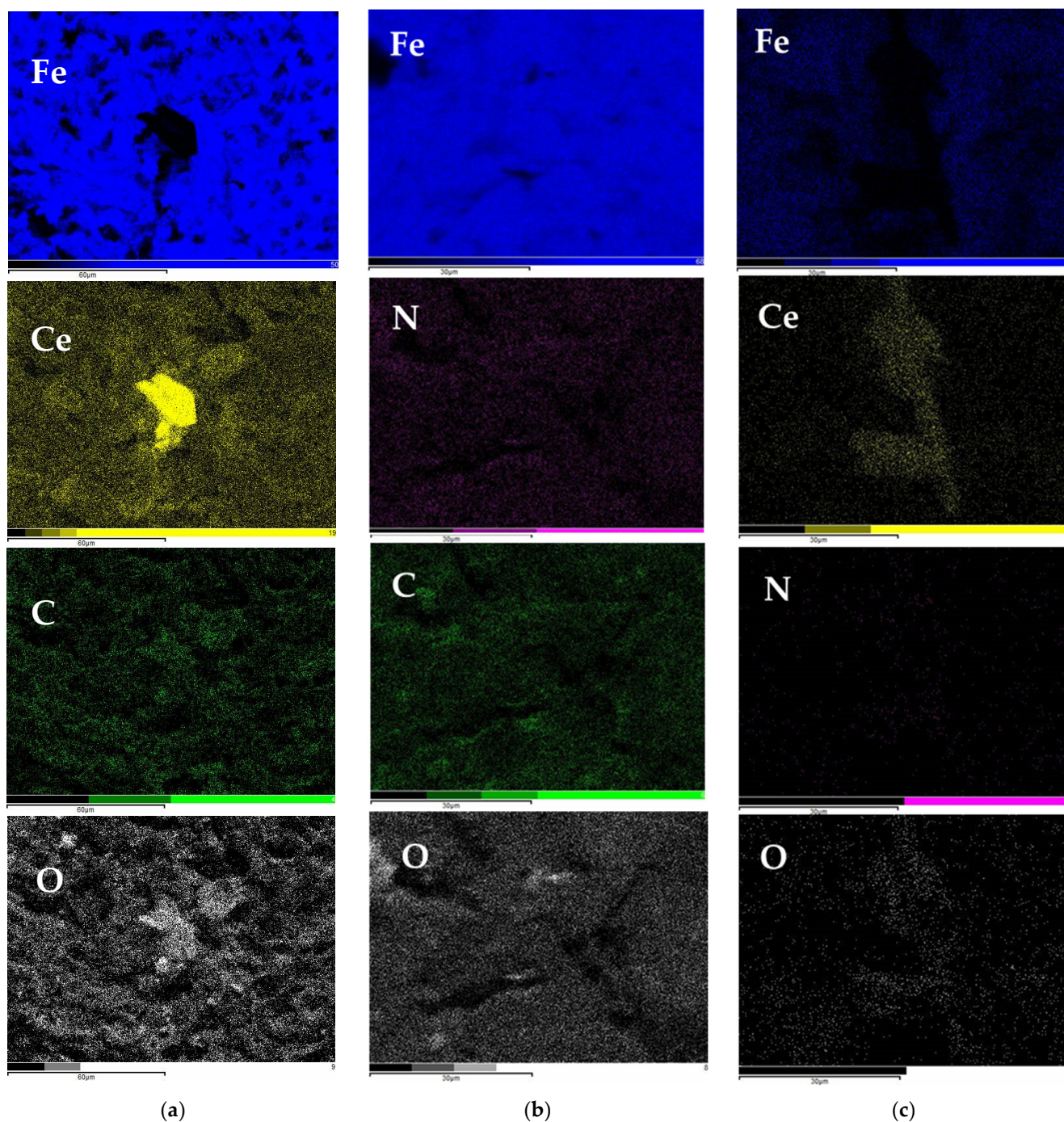


**Figure 12.** EDS mapping analysis of elements on carbon steel AISI 1018 surfaces after 72 h of exposure to a chloride–carbonate solution saturated with  $\text{CO}_2$  in the presence of (a)  $15 \text{ mg dm}^{-3}$   $\text{CeCl}_3$  (b)  $15 \text{ mg dm}^{-3}$  IOA and (c) the mixture of  $15 \text{ mg dm}^{-3}$   $\text{CeCl}_3$  and  $15 \text{ mg dm}^{-3}$  IOA.

A SEM image of the carbon steel surface after 72 h of exposure to the synthetic brine solution saturated with  $\text{CO}_2$  in the presence of  $15 \text{ mg dm}^{-3}$   $\text{CeCl}_3$  (Figure 11a) shows a porous and non-compact surface film. Such a surface is in accordance with the results obtained via the mass loss method (where the exposure to the tested electrolyte also lasts 72 h), whereby in the presence of  $\text{CeCl}_3$ , an inhibitory efficiency of 64.24% to 66.88% is achieved. EDS analysis and element mapping (Figure 12a) suggest that the formed thin film is a Ce–O–C compound, which according to XRD analysis (Figure 13), corresponds to cerium carbonate,  $\text{Ce}_2(\text{CO}_3)_3$ . The Raman spectrum for the system in the presence of

15 mg dm<sup>-3</sup> CeCl<sub>3</sub> (Figure 14a) suggests the existence of a symmetric stretching mode of the Ce–O vibrational unit at 454 cm<sup>-1</sup> [76].

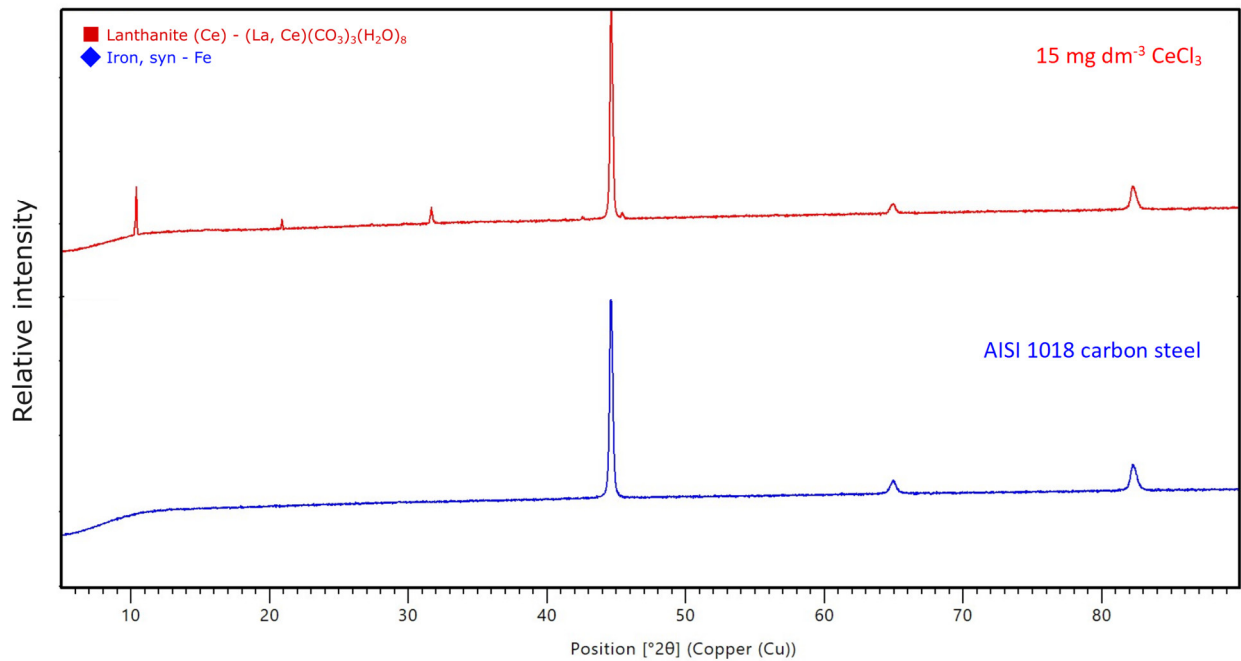


**Figure 13.** X-ray diffraction pattern of AISI 1018 carbon steel surface before and after exposure for 72 h to the synthetic brine solution saturated with CO<sub>2</sub> and with the addition of 15 mg dm<sup>-3</sup> CeCl<sub>3</sub>.

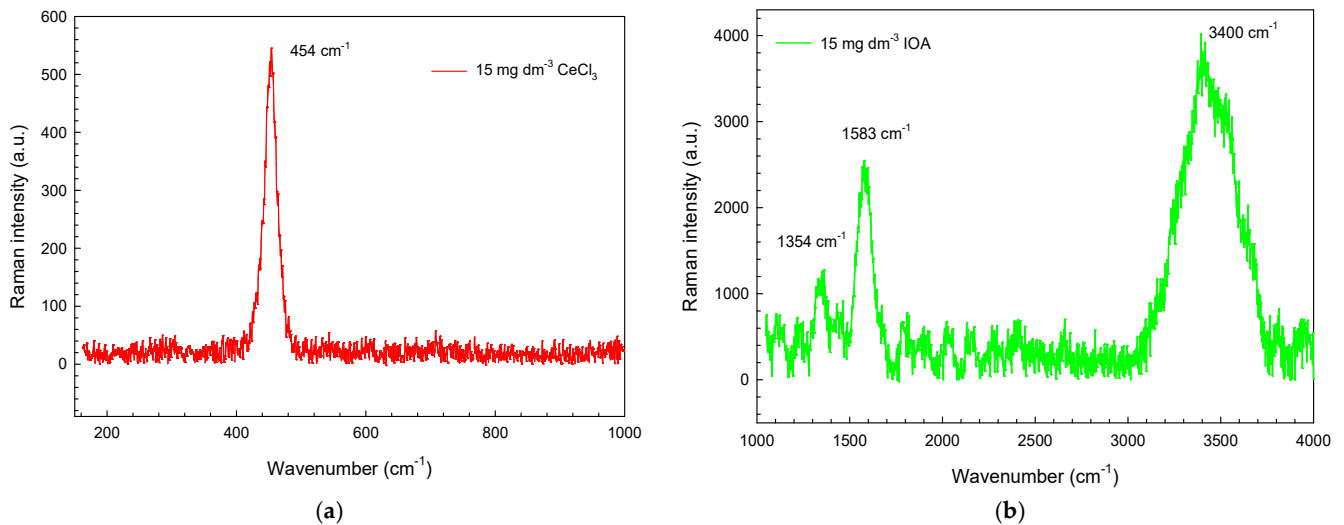
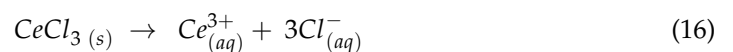
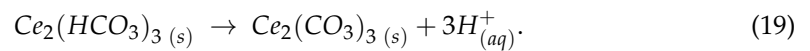
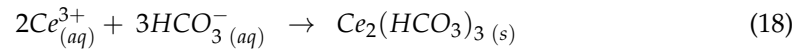


**Figure 14.** Raman spectra recorded on carbon steel AISI 1018 surfaces after 72 h of exposure to a chloride-carbonate solution saturated with CO<sub>2</sub> in the presence of (a) 15 mg dm<sup>-3</sup> CeCl<sub>3</sub> and (b) 15 mg dm<sup>-3</sup> IOA.

The formation of rare earth carbonates in CO<sub>2</sub> aqueous systems, with available CO<sub>3</sub><sup>2-</sup> ions, is thermodynamically favorable. The mechanism of formation corresponds to the process of capturing dissolved CO<sub>2</sub> near the metal surface, thereby reducing the corrosiveness of the medium [77–79]. The formation of cerium carbonate, Ce<sub>2</sub>(CO<sub>3</sub>)<sub>3</sub>, can be explained using the following reactions:



The carbonate anion comes from the dissociation of carbonic acid formed according to Equation (5). The dissociation of diprotic carbonic acid occurs in two steps. The first step (Equation (6)) is fast, while the second step (Equation (7)) is slower and occurs at approximately neutral pH. Therefore, it is assumed that the precipitation of cerium carbonate is analogous to the precipitation of iron carbonate in an acidic medium according to the following reactions [77,80]:



A SEM image of the carbon steel surface after 72 h of exposure to the synthetic brine solution saturated with CO<sub>2</sub> in the presence of 15 mg dm<sup>-3</sup> IOA (Figure 11b) shows a denser film compared to the surface layer in the presence of CeCl<sub>3</sub>. However, voids are observed, indicating that the layer does not have fully protective corrosion properties. The adsorption of imidazoline on the steel surface can be physical or chemical. In its molecular structure (Figure 2a), imidazoline has a heterocyclic ring with a double covalent bond ( $\pi$ -delocalized electrons) as well as free electron pairs on nitrogen atoms. These are also active sites through which IOA can be attached to the steel surface. In the case of chemisorption, it achieves a coordinative type of covalent bond in which it fills the empty d-orbitals of iron with its electrons, while in physical adsorption, an electrostatic interaction is achieved between the negatively charged part of the IOA molecule ( $\pi$ -electrons or free electron pairs on nitrogen) and the positively charged surface of the metal. Also, the hydrophobic hydrocarbon chain on the ring of the IOA molecule hinders the interaction of water molecules with the steel surface [40,81]. Adsorption through the active sites of the IOA molecule is confirmed by EDS element mapping (Figure 12b) and recorded Raman spectrum (Figure 14b). The Raman spectrum for pure IOA is shown in Figure 14b. The band at 1354 cm<sup>-1</sup> corresponds to C-N stretching, while the band at 1583 cm<sup>-1</sup> corresponds to N=C stretching in the heteroatomic ring [82,83]. The broad peak around 3400 cm<sup>-1</sup> represents the asymmetric O-H stretching region for water [84].

The SEM image of the steel surface after exposure to a mixture of CeCl<sub>3</sub> and IOA (Figure 11c) shows the existence of a dense and compact surface film. Low corrosion rates and high inhibitory effectiveness determined via the mass loss method after 72 h of exposure to a mixture of 15 mg dm<sup>-3</sup> IOA and 15 mg dm<sup>-3</sup> CeCl<sub>3</sub> prove that the film created in that time period has good protective properties. The Raman spectrum of the steel surface after exposure to the mixture of compounds (Figure 15) shows the existence of bands at around 1200 cm<sup>-1</sup> and 500 cm<sup>-1</sup>, which correspond to C-N stretching and Ce-O stretching, respectively [76,82,83]. The small shift in stretching modes compared to individual components is a consequence of the interaction of components adsorbed on the electrode surface. The improved/synergistic effect of the mixture of compounds and carbon steel surface layer after exposure to mixture can be explained by the pore plugging effect of cerium carbonate [85,86]. Cerium carbonate fills the pores of the IOA adsorbed film and makes the surface film more compact and with better protective properties.

Surface analyses showed the existence of protective films on the surface of carbon steel after 72 h of exposure to the system in the presence of individual components, CeCl<sub>3</sub> and IOA, as well as their mixtures. However, the protective properties of the film formed in the presence of compound mixtures are much better, as confirmed by the results obtained via the mass loss method. Electrochemical tests show high inhibitory efficiencies of individual compounds; however, since they were carried out after 24 h of exposure to the tested electrolytes, it is possible that their efficiency decreases with time. The mass loss test lasted for 72 h, after which the achieved inhibitory efficacies of the tested individual

compounds,  $\text{CeCl}_3$  and IOA, were significantly lower compared to the values obtained via electrochemical methods. The protective properties of the inhibitory layers of individual compounds decrease with time, possibly due to the desorption of the adsorbed inhibitor. Furthermore, the mixture of compounds showed synergistic action and better corrosion protection (lower corrosion rates and higher inhibitory efficacies) than the individual compounds. Cerium, as well as other rare earth elements, in combination with other compounds/coatings, is known for its so-called self-healing properties that depend on pH value and time [87,88]. Obviously, with longer exposure time, the porosity of the primary inhibitor film formed by IOA decreases, since the pores are filled with cerium carbonate. Such a layer is more compact and protects better against corrosion, but it is probably formed over a longer period (certainly more than 24 h).

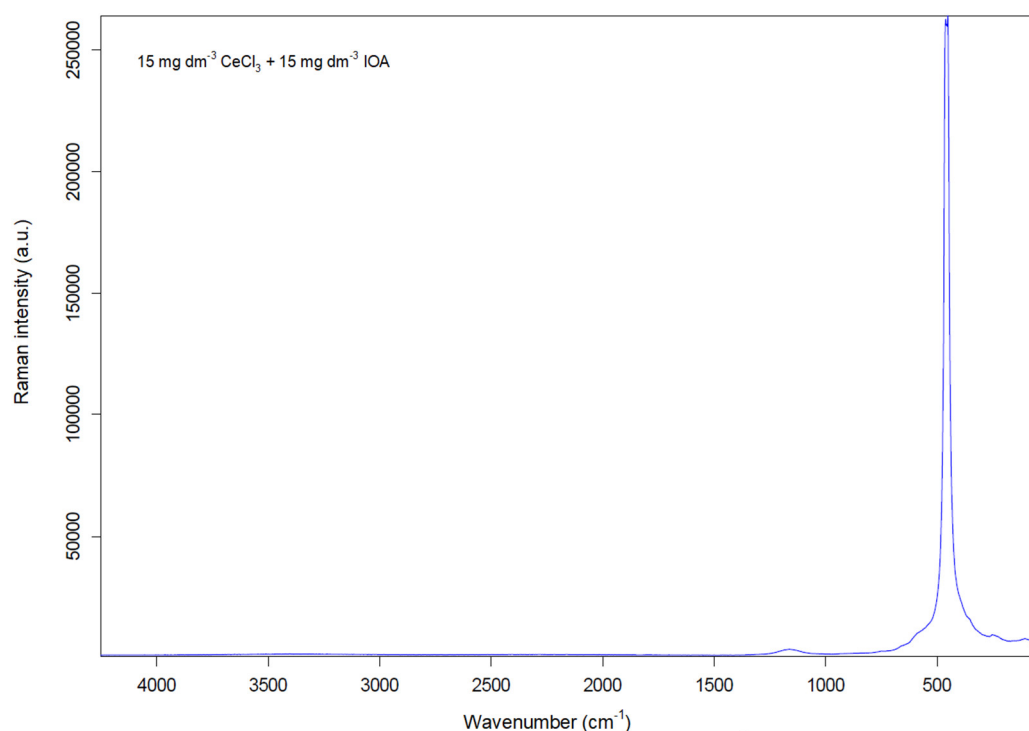


**Figure 15.** Raman spectra recorded on carbon steel AISI 1018 surfaces after 72 h of exposure to a chloride–carbonate solution saturated with  $\text{CO}_2$  in the presence of the mixture of  $15 \text{ mg dm}^{-3} \text{ CeCl}_3$  and  $15 \text{ mg dm}^{-3} \text{ IOA}$ .

#### 4. Conclusions

Based on the test results, for the sake of simplicity of this review, Table 5 shows the concentrations of individual components as well as the concentrations of the compound mixtures, where they achieve the lowest corrosion rates,  $v_{corr}$ , and the highest inhibitory efficacy,  $IE$ , (divided by test methods).

**Table 5.** Selected concentrations of individual components and their mixtures with the corresponding lowest corrosion rates and highest inhibitory efficiencies proven via individual testing methods.

System	Mass Loss Method			Linear Polarization			Potentiodynamic Polarization			EIS *	
	$\gamma$ ( $\text{mg dm}^{-3}$ )	$v_{corr}$ ( $\text{mm year}^{-1}$ )	$IE$ (%)	$\gamma$ ( $\text{mg dm}^{-3}$ )	$v_{corr}$ ( $\text{mm year}^{-1}$ )	$IE$ (%)	$\gamma$ ( $\text{mg dm}^{-3}$ )	$v_{corr}$ ( $\text{mm year}^{-1}$ )	$IE$ (%)	$\gamma$ ( $\text{mg dm}^{-3}$ )	$IE$ (%)
SBS	0	1.57	/	0	1.27	/	0	1.45	/	0	/
IOA	20	0.17	89.17	20	0.08	92.89	15	0.08	94.61	20	93.61
$\text{CeCl}_3$	10	0.52	66.88	20	0.06	95.65	15	0.05	96.27	20	90.96
$\text{CeCl}_3 + \text{IOA}$	15 + 15	0.05	96.82	15 + 15	0.03	97.94	15 + 15	0.03	97.78	10 + 15	94.92

\* The EIS method does not determine the corrosion rate.

- Mixtures of tested compounds, IOA and  $\text{CeCl}_3$ , showed mainly enhanced activity in corrosion protection compared to individual activity;
- Most of test methods showed that the mixture of compounds of  $15 \text{ mg dm}^{-3}$  IOA and  $15 \text{ mg dm}^{-3}$   $\text{CeCl}_3$  achieved the lowest corrosion rate ( $0.03 \text{ mm year}^{-1}$ – $0.05 \text{ mm year}^{-1}$ ) and the highest inhibitory efficiency (94.92%–97.94%);
- IOA can be categorized as an anodic corrosion inhibitor, while  $\text{CeCl}_3$  and the mixture of  $\text{CeCl}_3$  and IOA act as mixed corrosion inhibitors with a predominant influence on the anodic process;
- The inhibitory effect of individual components and their mixtures is realized by the formation of a protective film on the steel surface: IOA by its physical/chemical adsorption on the steel surface and  $\text{CeCl}_3$  by the formation of a protective layer of cerium carbonate, while the mixture of IOA and  $\text{CeCl}_3$  creates a porous layer of adsorbed IOA, with cerium carbonate filling these pores;
- The results obtained via the mass loss method and surface analysis can be considered more reliable compared to electrochemical tests since they provide information about the effectiveness and synergy of the compounds over a longer period (72 h) compared to electrochemical tests (24 h);
- According to results obtained via the mass loss method and surface analysis, the effectiveness of individual components decreases with time, but the effectiveness of mixtures of compounds is stable and high, and their synergistic action was determined;
- To gain a better insight into the inhibitory effect of the tested compounds and their synergy, electrochemical tests will be conducted in the future over a longer period; measurements will be carried out at different temperatures, and the nature of the adsorption of individual compounds and their mixtures will be determined.

**Author Contributions:** Conceptualization, T.B., G.B., K.Ž. and H.O.Ć.; Methodology, G.B.; Formal analysis, T.B., G.B., K.Ž. and H.O.Ć.; Investigation, T.B.; Resources, G.B. and T.B.; Writing—original draft preparation, T.B. and G.B.; Writing—review and editing, T.B., G.B., K.Ž. and H.O.Ć.; Visualization, T.B. and G.B.; Supervision, G.B., K.Ž. and H.O.Ć.; Project administration, G.B. and K.Ž.; Funding acquisition, K.Ž. All authors have read and agreed to the published version of the manuscript.

**Funding:** This research received no external funding.

**Institutional Review Board Statement:** Not applicable.

**Informed Consent Statement:** Not applicable.

**Data Availability Statement:** Data is contained within the article.

**Conflicts of Interest:** Author Tihomir Boriko was employed by INA, d.d. The remaining authors declare that the research was conducted in the absence of any commercial or financial relationships that could be construed as a potential conflict of interest.

## References

1. Sharifzadeh, M.; Triulzi, G.; Magee, C.L. Quantification of technological progress in greenhouse gas (GHG) capture and mitigation using patent data. *Energy Environ. Sci.* **2019**, *12*, 2789–2805. [[CrossRef](#)]
2. Gu, S.; Li, Y.; Teng, L.; Wang, C.; Hu, Q.; Zhang, D.; Ye, X.; Wang, J.; Iglauer, S. An experimental study on the flow characteristics during the leakage of high pressure  $\text{CO}_2$  pipelines. *Process Saf. Environ. Protect.* **2019**, *125*, 92–101. [[CrossRef](#)]
3. Jiang, K.; Ashworth, P. The development of Carbon Capture Utilization and Storage (CCUS) research in China: A bibliometric perspective. *Renew. Sustain. Energy Rev.* **2021**, *138*, 110521. [[CrossRef](#)]
4. Wang, C.; Li, Y.; Teng, L.; Gu, S.; Hu, Q.; Zhang, D.; Ye, X.; Wang, J. Experimental study on dispersion behavior during the leakage of high pressure  $\text{CO}_2$  pipelines. *Exp. Therm. Fluid Sci.* **2019**, *105*, 77–84. [[CrossRef](#)]
5. Ajayi, T.; Gomes, J.S.; Bera, A. A review of  $\text{CO}_2$  storage in geological formations emphasizing modeling, monitoring and capacity estimation approaches. *Petrol. Sci.* **2019**, *16*, 1028–1063. [[CrossRef](#)]

6. Xu, Z.X.; Li, S.Y.; Li, B.F.; Chen, D.Q.; Liu, Z.Y.; Li, Z.M. A review of development methods and EOR technologies for carbonate reservoirs. *Petrol. Sci.* **2020**, *17*, 990–1013. [CrossRef]
7. Hua, Y.; Shamsa, A.; Barker, R.; Neville, A. Protectiveness, morphology and composition of corrosion products formed on carbon steel in the presence of  $\text{Cl}^-$ ,  $\text{Ca}^{2+}$  and  $\text{Mg}^{2+}$  in high pressure  $\text{CO}_2$  environments. *Appl. Surf. Sci.* **2018**, *455*, 667–682. [CrossRef]
8. Li, Y.; Liu, X.; Wang, C.; Hu, Q.; Wang, J.; Ma, H.; Zhang, N. Research progress on corrosion behavior of gaseous  $\text{CO}_2$  transportation pipelines containing impurities. *Acta Metall. Sin.* **2020**, *57*, 283–294. [CrossRef]
9. Nestic, S. Effects of multiphase flow on internal  $\text{CO}_2$  corrosion of mild steel pipelines. *Energy Fuel.* **2012**, *26*, 4098–4111. [CrossRef]
10. Wang, Z.M.; Song, G.L.; Zhang, J. Corrosion Control in  $\text{CO}_2$  Enhanced Oil Recovery From a Perspective of Multiphase Fluids. *Front. Mater.* **2019**, *6*, 272. [CrossRef]
11. Yoon-Seok, C.; Nestic, S. Determining the corrosive potential of  $\text{CO}_2$  transport pipeline in high  $\text{pCO}_2$ -water environments. *Int. J. Greenh. Gas Control* **2011**, *5*, 788–797.
12. Xiang, Y. Corrosion issues of carbon capture, utilization, and storage. *Mater. Perform.* **2018**, *57*, 32–35.
13. Cao, S.; He, F.; Gao, J. Corrosion problems in the oil country tubular goods and their mitigation—A review. *Anti-Corros. Method M.* **2017**, *64*, 465–478. [CrossRef]
14. Obot, I.B.; Onyeachu, I.B.; Umoren, S.A.; Quraishi, M.A.; Sorour, A.A.; Chen, T.; Aljeaban, N.; Wang, Q. High temperature sweet corrosion and inhibition in the oil and gas industry: Progress, challenges and future perspectives. *J. Petrol. Sci. Eng.* **2020**, *185*, 106469. [CrossRef]
15. Onyeachu, I.B.; Chauhan, D.S.; Quraishi, M.A.; Obot, I.B. Influence of hydrodynamic condition on 1,3,5-tris(4-methoxyphenyl)-1,3,5-triazinane as a novel corrosion inhibitor formulation for oil and gas industry. *Corros. Eng. Sci. Technol.* **2021**, *56*, 154–161. [CrossRef]
16. Kermani, M.B.; Harrop, D. The impact of corrosion on oil and gas industry. *SPE Prod. Oper.* **1996**, *11*, 186–190. [CrossRef]
17. Kermani, B.M.; Morshed, A. Carbon dioxide corrosion in oil and gas production: A compendium. *Corrosion* **2003**, *59*, 659–683. [CrossRef]
18. Paolinelli, L.D.; Perez, T.; Simison, S.N. The effect of pre-corrosion and steel microstructure on inhibitor performance in  $\text{CO}_2$  corrosion. *Corros. Sci.* **2008**, *50*, 2456–2464. [CrossRef]
19. Sastri, V.S. *Green Corrosion Inhibitors: Theory and Practice*; John Wiley & Sons, Inc.: Hoboken, NJ, USA, 2011.
20. Darling, D.; Rakshpal, R. Green Chemistry Applied to Corrosion and Scale Inhibitors. In Proceedings of the CORROSION, San Diego, CA, USA, 22–27 March 1998; p. 98207.
21. Progress in Corrosion—The First 50 Years of the EFC, Edited by P. McIntyre & J. Vogelsang, Published for the European Federation of Corrosion by Maney Publishing on Behalf of the Institute of Materials, Minerals & Mining. 2009. Available online: <http://ndl.ethernet.edu.et/bitstream/123456789/64636/1/1371.pdf> (accessed on 16 October 2024.).
22. de Damborenea, J.; Conde, A.; Arenas, M.A. Corrosion inhibition with rare earth metal compounds in aqueous solutions. In *Rare Earth-Based Corrosion Inhibitors*; Woodhead Publishing: Cambridge, UK, 2014; pp. 84–116. [CrossRef]
23. Ahmed, M.A.; Amin, S.; Mohamed, A.A. Current and emerging trends of inorganic, organic and eco-friendly corrosion inhibitors. *RSC Adv.* **2024**, *14*, 31877–31920. [CrossRef]
24. Freiner, W.W. Review of Green Chemistry Corrosion Inhibitors for Aqueous Systems. In Proceedings of the 9th European Symposium on Corrosion Inhibitors, Ferrara, Italy, 4–8 September 2000; Universidad de Ferrara: Ferrara, Italy, 2000; Volume 1, pp. 1–37.
25. Satyanarayana Gupta, D.V. What is Green? In Proceedings of the CORROSION, San Diego, CA, USA, 22–27 March 1998; p. 206.
26. Hinton, B.R.W. Corrosion inhibition with rare earth metal salts. *J. Alloys Compd.* **1992**, *180*, 15–25. [CrossRef]
27. Mendez, J.A.; Vong, Y.M.; Bueno, J.d. Cerium and Other Rare Earth Salts as Corrosion Inhibitors—A Review. *Prot. Met. Phys. Chem. Surf.* **2022**, *58*, 801–810. [CrossRef]
28. Evans, C.H. *Biochemistry of the Lanthanides*; Springer Science + Business Media: New York, NY, USA, 1990.
29. Kawagoe, M.; Ishikawa, K.; Wang, S.C.; Yoshikawa, K.; Arany, S.; Zhou, X.P.; Wang, J.S.; Ueno, Y.; Koizumi, Y.; Kameda, T.; et al. Acute effects on the lung and the liver of oral administration of cerium chloride on adult, neonatal and fetal mice. *J. Trace Elem. Med. Biol.* **2008**, *22*, 59–65. [CrossRef] [PubMed]
30. Muecke, G.K.; Moller, P. The not- so rare earths. *Sci. Am.* **1988**, *258*, 72–77. [CrossRef]
31. Sastri, V.S.; Perumareddi, J.R.; Ramachandra Rao, V.; Rayudu, G.V.S.; Bünzli, J.C.G. *Modern Aspects of Rare Earths and Their Complexes*, 1st ed.; Elsevier Science: Amsterdam, The Netherlands, 2003.
32. Mohammedi, D.; Ismail, F.; Rehamnia, R.; Bensalem, R.; Savadogo, O. Corrosion behaviour of steel in the presence of rare earth salts: Synergistic effect. *Corros. Eng. Sci. Technol.* **2015**, *50*, 633–638. [CrossRef]
33. Bernal, S.; Botana, F.J.; Calvino, J.J.; Marcos, M.; Perez-Omil, J.A.; Vidal, H. Lanthanide salts as alternative corrosion inhibitors. *J. Alloys Compd.* **1995**, *225*, 638–641. [CrossRef]
34. Davó, B.; de Damborenea, J.J. Use of rare earth salts as electrochemical corrosion inhibitors for an Al–Li–Cu (8090) alloy in 3.56% NaCl. *Electrochim. Acta* **2004**, *49*, 4957–4965. [CrossRef]

35. Dastgheib, A.; Attar, M.M.; Zarebidaki, A. Evaluation of Corrosion Inhibition of Mild Steel in 3.5 wt% NaCl Solution by Cerium Nitrate. *Met. Mater. Int.* **2020**, *26*, 1634–1642. [[CrossRef](#)]
36. Chen, X.-B.; Cain, T.; Scully, J.R.; Birbilis, N. Technical Note: Experimental Survey of Corrosion Potentials for Rare Earth Metals Ce, Er, Gd, La, and Nd as a Function of pH and Chloride Concentration. *Corrosion* **2013**, *70*, 323–328. [[CrossRef](#)]
37. Arenas, M.A.; Conde, A.; de Damborenea, J.J. Cerium: A suitable green corrosion inhibitor for Tinplate. *Corros. Sci.* **2002**, *44*, 511–520. [[CrossRef](#)]
38. Okafor, P.C.; Liu, C.; Liu, X.; Zheng, Y.; Wang, F.; Lin, C.Y. Corrosion inhibition and adsorption behavior of imidazoline salt on N80 carbon steel in CO<sub>2</sub>-saturated solutions and its synergism with thiourea. *J. Solid State Electrochem.* **2010**, *14*, 1367–1376. [[CrossRef](#)]
39. Heydari, M.; Javidi, M. Corrosion inhibition and adsorption behaviour of an amido-imidazoline derivative on API 5L X52 steel in CO<sub>2</sub>-saturated solution and synergistic effect of iodide ions. *Corros. Sci.* **2012**, *61*, 148–155. [[CrossRef](#)]
40. Munis, A.; Zhao, T.; Zheng, M.; Rehman, A.U.; Wang, F. A newly synthesized green corrosion inhibitor imidazoline derivative for carbon steel in 7.5% NH<sub>4</sub>Cl solution. *Sustain. Chem. Pharm.* **2020**, *16*, 1000258. [[CrossRef](#)]
41. Zhao, J.; Duan, H.; Jiang, R. Synergistic corrosion inhibition effect of quinoline quaternary ammonium salt and Gemini surfactant in H<sub>2</sub>S and CO<sub>2</sub> saturated brine solution. *Corros. Sci.* **2015**, *91*, 108–119. [[CrossRef](#)]
42. Zhang, D.; Wu, H.; Gao, L. Synergistic inhibition effect of l-phenylalanine and rare earth Ce(IV) ion on the corrosion of copper in hydrochloric acid solution. *Mater. Chem. Phys.* **2012**, *133*, 981–986. [[CrossRef](#)]
43. Marcelin, S.; Pèbère, N. Synergistic effect between 8-hydroxyquinoline and benzotriazole for the corrosion protection of 2024 aluminium alloy: A local electrochemical impedance approach. *Corros. Sci.* **2015**, *101*, 66–74. [[CrossRef](#)]
44. Khamis, A.; Saleh, M.M.; Awad, M.I. Synergistic inhibitor effect of cetylpyridinium chloride and other halides on the corrosion of mild steel in 0.5 M H<sub>2</sub>SO<sub>4</sub>. *Corros. Sci.* **2013**, *66*, 343–349. [[CrossRef](#)]
45. Wang, Y.; Northwood, D.O. Effects of O<sub>2</sub> and H<sub>2</sub> on the corrosion of SS316L metallic bipolar plate materials in simulated anode and cathode environments of PEM fuel cells. *Electrochim. Acta* **2007**, *52*, 6793–6798. [[CrossRef](#)]
46. Bahrami, M.J.; Hosseini, S.M.A.; Pilvar, P. Experimental and theoretical investigation of organic compounds as inhibitors for mild steel corrosion in sulfuric acid medium. *Corros. Sci.* **2010**, *52*, 2793–2803. [[CrossRef](#)]
47. Elgaddafi, R.; Naidu, A.; Ahmed, R.; Shah, S.; Hassani, S.; Osisanya, S.O.; Saasen, A. Modeling and experimental study of CO<sub>2</sub> corrosion on carbon steel at elevated pressure and temperature. *J. Nat. Gas Sci. Eng.* **2015**, *27*, 1620–1629. [[CrossRef](#)]
48. Tan, J.; Guo, L.; Yang, H.; Zhang, F.; El Bakri, Y. Synergistic effect of potassium iodide and sodium dodecyl sulfonate on the corrosion inhibition of carbon steel in HCl medium: A combined experimental and theoretical investigation. *RSC Adv.* **2020**, *10*, 15163–15170. [[CrossRef](#)]
49. Li, X.; Deng, S.; Du, G.; Xie, X. Synergistic inhibition effect of walnut green husk extract and sodium lignosulfonate on the corrosion of cold rolled steel in phosphoric acid solution. *J. Taiwan Inst. Chem. Eng.* **2020**, *114*, 263–283. [[CrossRef](#)]
50. Wang, Z.; Wang, T.; Zhu, J.; Wei, L.; Shen, Y.; Li, N.; Hu, J. Synergistic effect and mechanism of copper corrosion inhibition using cinnamaldehyde and vanillin in HCl solution: An experimental and theoretical approach. *Colloids Surf. A Physicochem. Eng. Asp.* **2019**, *563*, 246–254. [[CrossRef](#)]
51. Pustaj, G.; Kapor, F.; Kvasnička, P. Inhibition properties and adsorption behavior of olive leaf extract on N80 carbon steel in CO<sub>2</sub>-saturated brine solution. *Int. J. Mater. Res.* **2014**, *105*, 992–998. [[CrossRef](#)]
52. Žbulj, K.; Bilić, G.; Simon, K.; Hrnčević, L. Lady's Mantle Flower as a Biodegradable Plant-Based Corrosion Inhibitor for CO<sub>2</sub> Carbon Steel Corrosion. *Coatings* **2024**, *14*, 671. [[CrossRef](#)]
53. Tran, T.; Brown, B.N.; Nescic, S. Corrosion of Mild Steel in an Aqueous CO<sub>2</sub> Environment—Basic Electrochemical Mechanisms Revisited. In Proceedings of the NACE—International Corrosion Conference Series 2015, Conference & Expo, Dallas, TX, USA, 15–19 March 2015. Paper No. 5671.
54. Kahyarian, A.; Nescic, S. On the mechanism of carbon dioxide corrosion of mild steel: Experimental investigation and mathematical modeling at elevated pressures and non-ideal solutions. *Corros. Sci.* **2020**, *173*, 108719. [[CrossRef](#)]
55. El-Katori, E.E.; Fouda, A.S.; Mohamed, R.R. Synergistic corrosion inhibition activity of the *Chicoriumintybus* extract and iodide ions for mild steel in acidic media. *J. Chil. Chem. Soc.* **2020**, *65*, 4672–4681. [[CrossRef](#)]
56. Rahayu, D.U.C.; Cahyani, S.; Abdullah, I.; Nurani, D.A.; Krisnandi, Y.K. Microwave-assisted synthesis of organic corrosion inhibitor based imidazoline-stearic. *IOP Conf. Ser. Mater. Sci. Eng.* **2019**, *902*, 012019. [[CrossRef](#)]
57. Porcayo-Calderon, J.; Canto, J.; Martinez de la Escalera, L.M.; Neri, A. Sweet Corrosion Inhibition by CO<sub>2</sub> Capture. *Molecules* **2022**, *27*, 5209. [[CrossRef](#)]
58. Martinez de la Escalera, D.M.; Ramos-Hernandez, J.J.; Porcayo-Palafox, E.; Porcayo-Calderon, J.; Gonzalez-Rodriguez, J.G.; Martinez-Gomez, L. Effect of Nd<sup>3+</sup> Ion Concentration on the Corrosion Resistance of API X70 Steel in Chloride-Rich Environments. *Adv. Mater. Sci. Eng.* **2018**, *2018*, 9328317. [[CrossRef](#)]

59. Porcayo-Calderon, J.; Ramos-Hernandez, J.J.; Porcayo-Palafox, E.; Martinez de la Escalera, L.M.; Canto, J.; Gonzalez-Rodriguez, J.G.; Martinez-Gomez, L. Sustainable Development of Corrosion Inhibitors from Electronic Scrap: Synthesis and Electrochemical Performance. *Adv. Mater. Sci. Eng.* **2019**, *2019*, 6753658. [CrossRef]
60. Zhang, G.; Chen, C.; Lu, M.; Chai, C.; Wu, Y. Evaluation of inhibition efficiency of an imidazoline derivative in CO<sub>2</sub>-containing aqueous solution. *Mater. Chem. Phys.* **2007**, *105*, 331–340. [CrossRef]
61. Lopez, D.A.; Simison, S.N.; de Sanchez, S.R. The influence of steel microstructure on CO<sub>2</sub> corrosion. EIS studies on the inhibition efficiency of benzimidazole. *Electrochem. Acta* **2003**, *48*, 845–854. [CrossRef]
62. Pustaj, G.; Kapor, F.; Jakovljević, S. Carbon dioxide corrosion of carbon steel and corrosion inhibition by natural olive leaf extract: Die Kohlendioxid-Korrosion von Kohlenstoffstahl und die Korrosionshemmung durch natürlichen Olivenblattextrakt. *Mater. Werkst.* **2017**, *48*, 122–138. [CrossRef]
63. Pustaj, G.; Kapor, F.; Veinović, Ž. Olive Leaf Extract as a Corrosion Inhibitor of Carbon Steel in CO<sub>2</sub>-Saturated Chloride–Carbonate Solution. *Int. J. Electrochem. Sci.* **2016**, *11*, 7811–7829. [CrossRef]
64. Herrera Hernández, H.; González Díaz, F.; Fajardo SanMiguel, G.; Velázquez Altamirano, J.C.; González Morán, C.O.; Morales Hernández, J. Electrochemical impedance spectroscopy as a practical tool for monitoring the carbonation process on reinforced concrete structures. *Arab. J. Sci. Eng.* **2019**, *44*, 10087–10103. [CrossRef]
65. Herrera Hernández, H.; Ruiz Reynoso, A.M.; Trinidad González, J.C.; Gonzales Moran, C.O.; Miranda Hernandez, J.G.; Mandujano Ruiz, A.; Morales Hernandez, J.; Orozco Cruz, R. Electrochemical Impedance Spectroscopy (EIS): A Review Study of Basic Aspects of the Corrosion Mechanism Applied to Steels. In *Electrochemical Impedance Spectroscopy*; IntechOpen: London, UK, 2020. [CrossRef]
66. Desimone, M.P.; Grundmeier, G.; Gordillo, G.; Simison, S.N. Amphiphilic amido-amine as an effective corrosion inhibitor for mild steel exposed to CO<sub>2</sub> saturated solution: Polarization, EIS and PM-IRRAS studies. *Electrochim. Acta* **2011**, *56*, 2990–2998. [CrossRef]
67. El-Azazy, M.; Mart, M.; Annus, P. (Eds.) *Electrochemical Impedance Spectroscopy*; IntechOpen: London, UK, 2020. [CrossRef]
68. Sun, J.B.; Zhang, G.A.; Liu, W.; Lu, M.X. The formation mechanism of corrosion scale and electrochemical characteristic of low alloy steel in carbon dioxide-saturated solution. *Corros. Sci.* **2012**, *57*, 131–138. [CrossRef]
69. Nam, N.D.; Bui, Q.V.; Mathesh, M.; Tan, M.Y.J.; Forsyth, M. A study of 4-carboxyphenylboronic acid as a corrosion inhibitor for steel in carbon dioxide containing environments. *Corros. Sci.* **2013**, *76*, 257–266. [CrossRef]
70. Singh, A.K.; Quraishi, M.A. Effect of Cefazolin on the corrosion of mild steel in HCl solution. *Corros. Sci.* **2010**, *52*, 152–160. [CrossRef]
71. Jia, W. A study on the impedance responses of inhibitor desorption. *Chin. J. Ocean. Limnol.* **1998**, *16*, 54–59. [CrossRef]
72. Okafor, P.C.; Liu, X.; Zheng, Y. Corrosion inhibition of mild steel by ethylamino imidazoline derivative in CO<sub>2</sub>-saturated solution. *Corros. Sci.* **2009**, *51*, 761–768. [CrossRef]
73. Videm, K. The Anodic Behavior of Iron and Steel in Aqueous Solutions with CO<sub>2</sub>, HCO<sub>3</sub><sup>−</sup>, CO<sub>3</sub><sup>2−</sup> and Cl<sup>−</sup>. In Proceedings of the CORROSION, Orlando, FL, USA, 26–31 March 2000; p. 39.
74. Li, L.J.; Zhang, X.P.; Lei, J.L.; Pan, F.S. Osmanthus Fragran Leaves Extract as Corrosion Inhibitor for Carbon Steel in Hydrochloric Acid Solution. *Asian J. Chem.* **2012**, *24*, 1649–1653.
75. Bentiss, F.; Lebrini, M.; Vezin, H.; Chai, F.; Traisnel, M.; Lagrené, M. Enhanced corrosion resistance of carbon steel in normal sulfuric acid medium by some macrocyclic polyether compounds containing a 1,3,4-thiadiazole moiety: AC impedance and computational studies. *Corros. Sci.* **2009**, *51*, 2165–2173. [CrossRef]
76. Kim, N.W.; Lee, D.K.; Yu, H. Selective shape control of cerium oxide nanocrystals for photocatalytic and chemical sensing effect. *RSC Adv* **2019**, *9*, 13829–13837. [CrossRef]
77. Anadebe, V.C.; Chukwuike, V.I.; Ramanathan, S.; Barik, R.C. Cerium-based metal organic framework (Ce-MOF) as corrosion inhibitor for API 5L X65 steel in CO<sub>2</sub>- saturated brine solution: XPS, DFT/MD-simulation, and machine learning model prediction. *Process Saf. Environ. Prot.* **2022**, *168*, 499–512. [CrossRef]
78. Hassas, B.V.; Rezaee, M.; Pisupati, S.V. Precipitation of rare earth elements from acid mine drainage by CO<sub>2</sub> mineralization process. *Chem. Eng. J.* **2020**, *399*, 125716. [CrossRef]
79. Pei, S.-L.; Pan, S.-Y.; Li, Y.-M.; Chiang, P.-C. Environmental benefit assessment for the carbonation process of petroleum coke fly ash in a rotating packed bed. *Environ. Sci. Technol.* **2017**, *51*, 10674–10681. [CrossRef]
80. Barker, R.; Burkle, D.; Charpentier, T.; Thompson, H.; Neville, A. A review of iron carbonate (FeCO<sub>3</sub>) formation in the oil and gas industry. *Corros. Sci.* **2018**, *142*, 312–341. [CrossRef]
81. Tyagi, R.; Tyagi, V.K.; Pandey, S.K. Imidazoline and Its Derivatives: An Overview. *J. Oleo Sci.* **2007**, *56*, 211–222. [CrossRef]
82. Shimpi, M.R.; Childs, S.L.; Bostrom, D.; Velaga, S.P. New cocrystals of ezetimibe with l-proline and imidazole. *CrystEngComm* **2014**, *16*, 8984–8993. [CrossRef]
83. Raman Band Correlation Table. Available online: <https://www.chem.uci.edu/~dmitryf/manuals/Raman%20correlations.pdf> (accessed on 10 December 2024).

84. Durickovic, I. Using Raman Spectroscopy for Characterization of Aqueous Media and Quantification of Species in Aqueous Solution. In *Applications of Molecular Spectroscopy to Current Research in the Chemical and Biological Sciences*; Stauffer, M.T., Ed.; InTech: London, UK, 2016. [[CrossRef](#)]
85. Penga, Y.; Hughes, A.E.; Mardel, J.I.; Deacon, G.B.; Junk, P.C.; Catubig, R.A.; Forsyth, M.; Hinton, B.R.W.; Somers, A.E. Dual function of rare earth carboxylate compounds on the barrier properties and active corrosion inhibition of epoxy coatings on mild steel. *Prog. Org. Coat.* **2023**, *185*, 107870. [[CrossRef](#)]
86. Ivušić, F.; Lahodny-Šarc, O.; Otmačić Ćurković, H.; Alar, V. Synergistic inhibition of carbon steel corrosion in seawater by cerium chloride and sodium gluconate. *Corros. Sci.* **2015**, *98*, 88–97. [[CrossRef](#)]
87. Habib, S.; Fayyad, E.; Nawaz, M.; Khan, A.; Shakoor, R.A.; Kahraman, R.; Abdullah, A. Cerium Dioxide Nanoparticles as Smart Carriers for Self-Healing Coatings. *Nanomaterials* **2020**, *10*, 791. [[CrossRef](#)] [[PubMed](#)]
88. Guergova, D.; Stoyanova, E.; Stoychev, D.; Avramova, I.; Stefanov, P. Self-healing effect of ceria electrodeposited thin films on stainless steel in aggressive 0.5 mol/L NaCl aqueous solution. *J. Rare Earths* **2015**, *33*, 1212–1227. [[CrossRef](#)]

**Disclaimer/Publisher’s Note:** The statements, opinions and data contained in all publications are solely those of the individual author(s) and contributor(s) and not of MDPI and/or the editor(s). MDPI and/or the editor(s) disclaim responsibility for any injury to people or property resulting from any ideas, methods, instructions or products referred to in the content.